February 1, 2016

Evaluating and Extending the Ocean Wind Climate Data Record

Prepared for:

Earth Science Division

NASA Headquarters

Prepared by:

Ocean Vector Wind Science Team (OVWST)

Climate Working Group

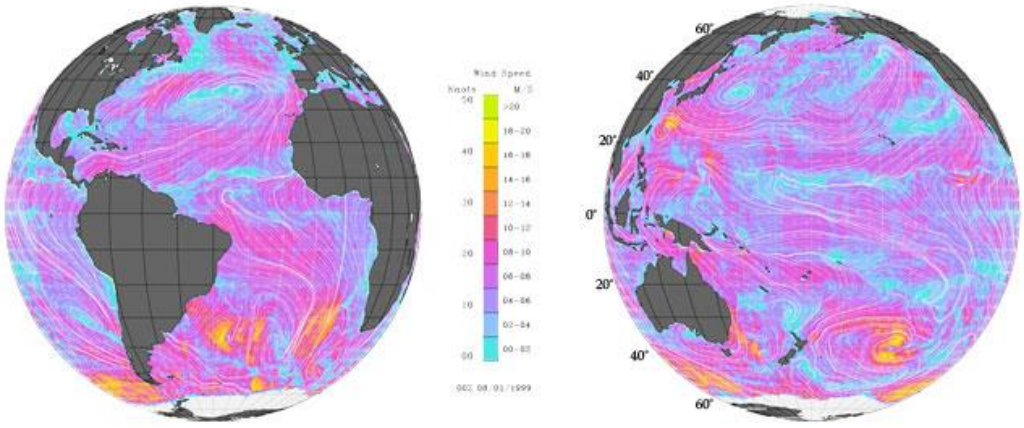

Acknowledgments

This Report was prepared under the auspices of the NASA's Ocean Vector Wind Science Team (OVWST) Climate Working Group. The following scientists contributed to this Report.

Brigham Young University
David Long

Florida State University (FSU)
Mark Bourassa, FSU

Jet Propulsion Laboratory (JPL)
Ernesto Rodriguez, Bryan Stiles, Robert Gaston, Alexander Fore, Sermsak Jaruwatanadilok, Svetla Hristova Veleva, Joe Turk, Lee Poulsen, Douglas Tyler

National Oceanic and Atmospheric Administration (NOAA)
Ross Hoffman

Oregon State University (OSU)
Larry O'Neill

Remote Sensing Systems (RSS)
Lucrezia Ricciardulli and Deborah K. Smith

Royal Netherlands Meteorological Institute (KNMI)
Ad Stoffelen and Anton Verhoef

University of New Hampshire
Douglas Vandemark

Woods Hole Oceanographic Institution (WHOI)
Tom Farrar

In addition, Eric Lindstrom at NASA Headquarters gave advice on the scope of the Report.

Thank you all for helping to bring this together,

Frank J. Wentz, Remote Sensing Systems
Editor: *Evaluating and Extending the Ocean Wind Climate Data Record*
Co-Chair: OVWST Climate Working Group

Executive Summary

Satellite sensors have been systematically measuring near-surface ocean winds for nearly 30 years, establishing an important legacy in studying and monitoring weather and climate variability. These wind measurements come from 18 passive microwave radiometers, which only provide wind speed, and 10 active microwave scatterometers, which provide both speed and direction. These 28 sensors taken together and properly intercalibrated provide a highly accurate depiction of oceanic winds over the last 3 decades. This report provides a plan for evaluating the existing ocean wind climate data record (OW-CDR) and extending this record into the future.

Given the large number of sensors, the existing OW-CDR is robust. Except for early in the record, there have been multiple satellite sensors in operation, allowing comparisons between satellites for CDR validation. This 30-year archive of wind datasets needs to be maintained and periodically updated.

Looking to the future, ESA and ISRO have made commitments to continue wind scatterometry, but the same cannot be said for the continuation of microwave radiometers. The possible end of the 30-year wind speed record from spaceborne radiometers is of considerable concern. Currently there are no commitments for follow-on sensors to WindSat, AMSR-2, or GMI. The only scheduled radiometer, other than from China or Russia, is the second-generation MetOp microwave imager (MWI), which will have limited wind-sensing capabilities and will not launch before 2022.

The need for absolute wind calibration via ocean buoys will continue into the future. Satellite wind sensors are not perfectly stable, and now that the time series of the OW-CDR is 3 decades, one must be concerned about small drifts (≈0.1 m/s) over 30 years. Buoys are indispensable in validating these decadal records of satellite winds. In this regard, requirements for buoy calibration (number and locations) need to be quantified and communicated to the TPOS 2020 Project.

Now that there are multiple versions of the OW-CDR at different institutions, the opportunity arises to compare these datasets with the objective of evaluating the uncertainties associated with the construction of an OW-CDR. An OW Intercomparison Project will be formed as part of the OVWST Climate Working Group to initiate these studies.

There are a number of methods for extending the OW-CDR into the future, including direct Ku-band σ_o intercalibration (QuikScat/RapidScat ➔ ScatSat), multi-sensor wind speed intercalibration (ASCAT-A&B/WindSat/AMSR2/GMI ➔ScatSat), and stable rain forest targets. All of these calibration methods will be used, with the possible exception of QuikScat. QuikScat will add value to the OW-CDR calibration process. In addition, it provides the means to continue the time series of Ku-band σ_o measurements over land and ice. However, this will require extending the QuikScat mission through 2016 and possibly into 2017.

RapidScat is the only vector wind sensor that views the ocean throughout the complete 24-hour diurnal cycle. This unique capability has great potential for (1) cross-calibrating sun-synchronous sensors and (2) characterizing the diurnal variability of winds over the world's oceans. While there are other methods for cross-calibrating sun-synchronous sensors, there is no substitute for the diurnal vector wind information coming from RapidScat. It is too soon to understand the full implications of RapidScat's gain anomaly. However, given its unique diurnal capabilities, effort should be directed towards overcoming the gain anomaly and extracting as much information as possible from this sensor.

Specialized model assimilations offer the prospect of mitigating the long-standing problem of constructing a composite OW-CDR from multiple satellites viewing the Earth at different local times. The challenge is to remap the winds on a regularly spaced temporal/spatial grid while preserving the satellite wind information. Research should be focused on meeting this challenge.

Table of Contents

1. Introduction

The climate data record (CDR) for ocean vector winds (OVW) begins in 1991 with the scatterometer flown by the European Space Agency (ESA) onboard its European Remote Sensing Satellite-1 (ERS-1). Since then, NASA, ESA, the Indian Space Research Organization (ISRO), and China National Space Administration (CNSA) have flown 10 scatterometers. Currently there are 5 scatterometers in operation: ASCAT-A on MetOp-A and ASCAT-B on MetOp-B, SeaWinds on QuikScat, RapidScat on the ISS, and SCAT on the CNSA HY-2A. However, the QuikScat spin mechanism failed in November 2009, and the sensor now operates only in a fixed non-spinning mode. In the near future, the OVW-CDR will contain data from two new scatterometers: ISRO's ScatSat (estimated launch mid-2016) and ESA's ASCAT-C on MetOp-C (estimated launch 2018). The OVW-CDR also contains vector wind retrievals from WindSat, which is the only passive radiometer with wind direction capabilities due to its polarimetric channels.

In addition to the OVW-CDR, there is also a wind-speed-only CDR provided by satellite microwave imaging radiometers. This ocean wind speed (OWS) CDR dates back to 1987 with the launch of the first Special Sensor Microwave Imager (SSM/I) and now consists of observations from 18 microwave radiometers. For completeness, the wind speed retrievals from the scatterometers are also included in the OWS-CDR. The accuracies of scatterometer and radiometer wind speeds are very similar despite the different measurement technologies. When referring to both the OVW-CDR and OWS-CDR, we simply use the term OW-CDR (ocean wind).

Several institutions, including the Jet Propulsion Laboratory (JPL), the Royal Netherlands Meteorological Institute (KNMI), and Remote Sensing Systems (RSS), have produced OW-CDRs for various subsets of satellite wind sensors. Section 2 gives the status of these CDRs and stresses the importance of maintaining and updating the older datasets. Section 2 also points to the challenge of constructing a composite OW-CDR from multiple satellites viewing the Earth at different local times. One solution is to use numerical assimilation models to account for the diurnal cycle. This is further discussed in Section 5.

Section 3 discusses various ways of evaluating the OW-CDRs including comparisons with winds from ocean buoys and numerical weather forecast models. This section also emphasizes the importance of having consistent winds from sensors on different satellites. The section concludes with a plan for comparing OVW datasets from different institutions. An OVW Intercomparison Project is described with the objective of evaluating the uncertainties associated with the construction of an OVW-CDR. A better appreciation of the uncertainties is expected to lead to improvements in the OVW-CDR.

Section 4 gives various strategies for extending the OW-CDR into the future using the large array of wind sensors currently in operation. The focus is on integrating ScatSat in the OVW-CDR. The direct intercalibration of Ku-Band σ_o measurements using the QuikScat/RapidScat ➔ ScatSat path is described along with the implications of QuikScat being in a non-spinning mode and the RapidScat gain anomaly that occurred in August 2015. A multi-sensor wind-speed intercalibration is also described along with examples of how this technique has been used in the past. For this method, calibration offsets are applied the ScatSat σ_o measurements to match the wind speed retrievals from ASCAT-A&B, WindSat, AMSR2, and GMI. The calibration of ScatSat Ku-band σ_o measurements using stable rain forest targets is also discussed. All of these calibration methods will be used, with the possible exception of QuikScat. The extension of the QuikScat mission is currently under consideration.

Section 5 discusses specialized assimilation models designed to provide vector winds on a regular temporal and spatial grid while retaining the satellite wind information. These assimilations offer the prospect of mitigating the long-standing problem of constructing a composite OW-CDR from multiple

satellites viewing the Earth at different local times. In this pursuit, RapidScat's unique capability of observing ocean winds over the complete 24-hour diurnal cycle will provide needed information. Re-mapping the winds on a regularly spaced temporal/spatial grid while maintaining the satellite wind information is clearly a challenge that needs addressing.

The Appendix provides a technical assessment of the performance of QuikScat in the non-spinning mode and RapidScat both before and after the gain anomaly. The QuikScat/RapidScat ➔ ScatSat σ_o calibration path is assessed.

2. Current Status of OW-CDRs

2.1 Existing Radiometer OWS and Scatterometer OVW Datasets

Systematic satellite measurements of ocean wind speeds (OWS) began in 1987 with the launch of the first SSM/I that flew on the DMSP F08 spacecraft. Since then an additional 17 satellite microwave imagers have gone into operation, as shown in Figure 2.1 and Table 2.1a. Currently there are 9 radiometers in operation: the SSMI/SSMIS on DMSP platforms F15 through F19, WindSat, AMSR2, GMI, and SMAP.

The time series of ocean vector winds (OVW) satellite measurements began in 1991 with the ESA scatterometer onboard the ERS-). Since then, NASA, ESA, ISRO, and CNSA have flown 10 scatterometers, as shown in Figure 2.1 and Table 2.1b. Currently there are 5 scatterometers in operation: ASCAT A&B, QuikScat, RapidScat, and SCAT. However, the QuikScat spin mechanism failed in November 2009, and the sensor only operates in a fixed non-spinning mode. Three future scatterometers are planned: ISRO's OSCAT sensor on ScatSat-1 (estimated launch mid-2016), SCAT on HY-2B (estimated launch 2017), and ESA's ASCAT sensor on MetOp-C (estimated launch 2018). To distinguish between the OSCAT on OceaSat-2 and the OSCAT on ScatSat-1, we use the name ScatSat when referring to the OSCAT on ScatSat-1 satellite within this document.

The construction of OW-CDRs from the large array of satellite wind datasets requires careful intercalibration and an assessment of long-term stability for each sensor. With respect to the radiometer datasets, all 18 microwave imagers (with the exception of the F18 and F19 SSMIS) have been intercalibrated and now constitute a 30-year climate record of ocean wind speeds (Wentz, 2013; Wentz, 2015; Wentz and Draper, 2016). In addition, the QuikScat and ASCAT-A wind speeds have recently been added to this OWS-CDR.

Similar efforts are underway to construct a complete OVW-CDR for the scatterometers extending from ERS-1 to present (Wentz and Ricciardulli, 2013; Ricciardulli and Wentz, 2015; Stoffelen et al., 2015). There currently exists partial OVW-CDRs consisting of QuikScat and ASCAT-A extending from 1999 to present available at:

RSS: www.remss.com/missions/QSCAT; www.remss.com/missions/ASCAT
KNMI:http://projects.knmi.nl/scatterometer/qscat_prod/http://projects.knmi.nl/scatterometer/archived_prod/

Whereas EUMETSAT and ISRO have made definite commitments to continue wind scatterometers into the future, the same cannot be said for the microwave radiometer wind sensors. The only scheduled sensor, other than from China or Russia, is the microwave imager (MWI) for the second-generation MetOp, which is scheduled to launch around 2022. MWI primary wind sensing channel is 31 GHz, which is less sensitive to wind than the 37 GHz used by previous wind sensors. Currently, there are no commitments for follow-on sensors to WindSat, AMSR2, or GMI.

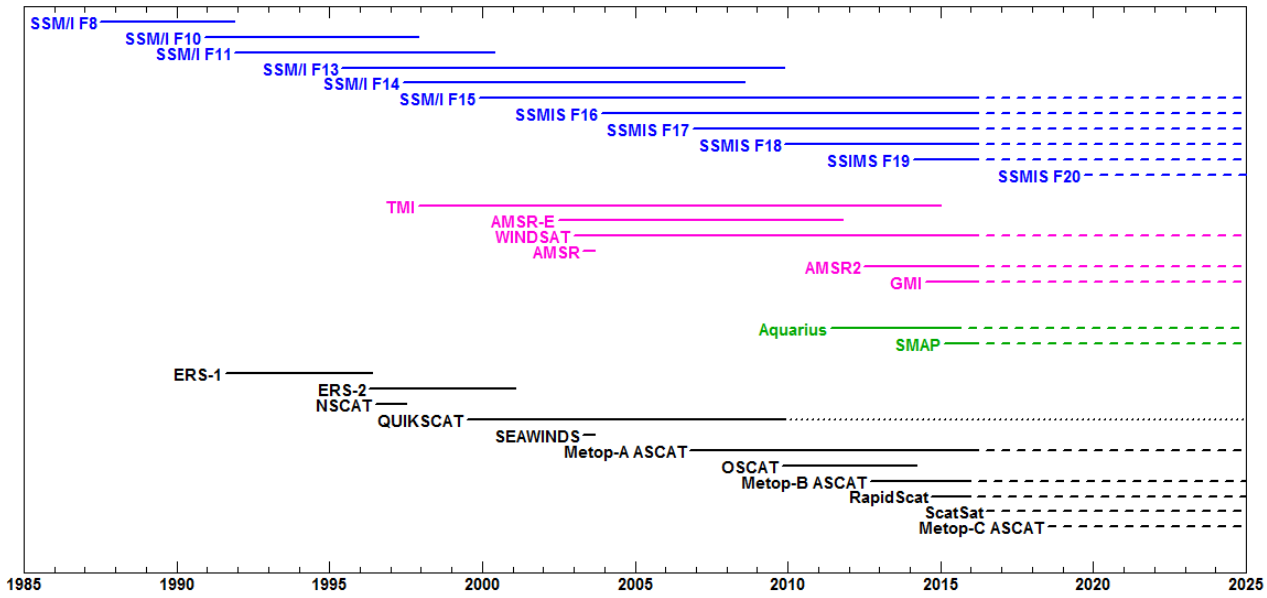

Figure 2.1. Three decades of satellite wind measurements. The black lines show the series of microwave scatterometers that provide ocean vector winds (OVW), including the upcoming ScatSat and ASCAT-C instruments. The dotted line extending the QuikScat from 2009 onward denotes the non-rotating phase of operation. There are no immediate plans to include the CNSA scatterometers in the OVW-CDR, and hence they are not included in this figure. The blue lines show the SSM/I and SSMIS instruments flown on the series of DMSP satellite platforms numbered F8 to F20. Currently, sensors on F15, F16, F17, F18 and F19 are in operation. These sensors only provide ocean wind speed, not direction. The pink lines show the microwave radiometers with the lower frequency channels needed for measuring sea surface temperatures in addition to wind speed, water vapor, clouds and rain rates. The lower frequency channels also improve the wind speed accuracy. WindSat on Coriolis, AMSR2 on GCOM-W1, and GMI on GPM are currently in operation. WindSat is the only microwave radiometer that also provides wind direction due to the inclusion of polarimetric channels. The green lines show the L-band radiometers Aquarius and SMAP, which are especially well suited for measuring high winds in storms.

This report does not consider the wind speed retrievals from satellite altimeters. The reason is the altimeter swath is very narrow (≈5 km) compared to the imaging radiometers that have swaths between 1000 and 1400 km. Thus, the altimeter spatial sampling is much less. However, the altimeter wind-speed record begins in 1991 and continues to present, overlapping much of the OWS-CDR from the microwave imagers. Hence, there is the opportunity to compare the two datasets for evaluation purposes. An initial comparison of an altimeter OWS-CDR produced by Young et al. (2011a) with the SSM/I OWS-CDR (Wentz et al., 2007) showed a large discrepancy, with the altimeter wind trends being 2.5 to 5 times higher than those reported elsewhere (Wentz and Ricciardulli, 2011; Young et al., 2011b). It is unclear if this large discrepancy is due to an inherent signal-to-noise problem in retrieving altimeter winds or if it is due to correctable problems in the construction of the altimeter OWS-CDR.

Table 2.1a. Current Radiometer Wind Speed Datasets

Instrument	Document Reference	Time Period	Production Institutions
F08 SSM/I	F08	Jul 1987 – Dec 1991	RSS
F10 SSM/I	F10	Dec 1990 – Nov 1997	RSS
F11 SSM/I	F11	Dec 1991 – May 2000	RSS
F13 SSM/I	F13	May 1995 – Nov 2009	RSS
F14 SSM/I	F14	May 1997 – Aug 2008	RSS
F15 SSM/I	F15	Dec 1999 – present	RSS
F16 SSMIS	F16	Oct 2003 – present	RSS
F17 SSMIS	F17	Dec 2006 – present	RSS
F18 SSMIS	F18	Oct 2009 – present	
F19 SSMIS	F19	Apr 2014 – present	
TRMM TMI	TMI	Nov 1997 – Apr 2015	RSS
ADEOS-II AMSR	AMSR	Dec 2002 – Oct 2003	RSS, JAXA
AQUA AMSR-E	AMSRE	May 2002 – Oct 2011	RSS, JAXA
GCOM-W1 AMSR2	AMSR2	May 2012 – present	RSS, JAXA
Coriolis WindSat	WindSat	Jan 2003 – present	RSS, NRL
GPM GMI	GMI	Feb 2014 – present	RSS
Aquarius	Aquarius	Jun 2011 – Jun 2015	RSS, JPL
SMAP	SMAP	Jan 2015 - present	RSS, JPL

Table 2.1b. Current and Future Scatterometer Vector Wind Datasets

Instrument	Document Reference	Time Period	Production Institutions
ERS-1 AMI-SCAT	ERS-1	Jul 1991 – Apr 1996	ESA
ERS-2 AMI-SCAT	ERS-2	Apr 1995 – Jun 2003	ESA
ADEOS-I NSCAT	NSCAT	Sep 1996 – Jun 1997	JPL, RSS
ADEOS-II SeaWinds	SeaWinds	Dec 2002 – Oct 2003	JPL, RSS
QuikScat SeaWinds	QuikScat	Jun 1999 – Nov 2009	JPL, RSS, KNMI
Metop-A ASCAT	ASCAT-A	Oct 2006 – present	KNMI, RSS
Metop-B ASCAT	ASCAT-B	Sep 2012 - present	KNMI
Metop-C ASCAT	ASCAT-C	2018 (planned)	
ISS RapidScat	RapidScat	Oct 2014 - present	JPL
Oceansat-2 OSCAT	Oceansat-2	Sep 2009 – Feb 2014	ISRO, KNMI
ScatSat-1 OSCAT	ScatSat	Jun 2016 (planned)	

2.2 Maintaining and Updating the Older OW Datasets

As we enter the 4th decade of satellite wind measurements, the timeline is becoming long enough to characterize the low-frequency decadal oscillations in ocean winds that drive the regional and global exchanges of moisture, momentum, and energy between the planet's oceans and atmosphere. The older OW datasets, some going back 30 years, need to be actively maintained and periodically improved else the scientific value of these historical datasets will become obscure and loose value relative to newly produced datasets. While making the wind datasets available from a NASA data center (i.e., a DAAC) is a good first step, more is required. Proactive encouragement and support for version updates and scientific advocacy are needed. By scientific advocacy, we mean explaining and demonstrating the value of these older data to the Earth Science Community at large. Without version updates and advocacy the older datasets lose consistency with newer datasets, and the value of the combined datasets will be little better than the sum of the components. Instead, we need the sum of the components to have greater value, resulting from consistent datasets useful for long-term studies.

As time goes on, we will better understand how to extract more information from the past and present scatterometer/radiometer measurements. Improved geophysical model functions (GMF) with extended parametrizations will be developed, and more advanced inverse methods (i.e., retrieval algorithms) will be derived. The current lack of proper error characterization of the wind retrievals needs to be remedied. By incorporating more ancillary data (satellite-inferred precipitation, sea-surface temperature, wave-height) into the retrieval process, the vector wind accuracy will improve. The implementation of these refinements and extensions will require widely publicized version updates, reprocessing, and scientific advocacy on a regular basis of every 3 to 5 years.

The fidelity of satellite intercalibration will also improve with time. We are just beginning to understand the characterization of the wind diurnal cycle using RapidScat and the TMI and GMI radiometers, all flying in rapidly precessing orbits that sample the full 24-hour cycle. The precise removal of small biases between sensors and the detection of slight sensor drifts are improving the extent to which we can now see subtle changes in our climate that are not easily discernable from in situ data.

The realization of all these potentials requires establishing a programmatic support mechanism that is focused on maintaining and improving the 30-year archive of satellite winds.

2.3 OW-CDR Dependence on the Diurnal Cycle

It is well known that ocean winds exhibit significant diurnal variability (Gille et al., 2003; Gille, 2005; Ueyama and Deser, 2008; Wood et al., 2009). When intercalibrating wind sensors on different platforms, this diurnal variation needs to be accounted for, as discussed in Section 3.5. Otherwise, true differences in the wind field due to the diurnal cycle will be misinterpreted as sensor calibration errors. Wind sensors that fly in low inclinations orbits, such as TMI, GMI, and RapidScat, can be used to connect the sun-synchronous sensors that observe the oceans at different local times. Using TMI, GMI, and RapidScat , 1-hour collocations can be obtained with each sun-synchronous sensors.

The fact that there are methods for handling diurnal variability for the purpose of sensor intercalibration does not solve the more fundamental problem of how to incorporate diurnal variability into the OW-CDR. For example, assuming QuikScat and ASCAT-A are perfectly intercalibrated from a sensor standpoint, the wind fields from the two sensors are still inconsistent in that they are at four different times of day (6 am and 6 pm for QuikScat; 9:30 am and 9:30 pm for ASCAT). This situation gets murkier at the higher latitudes where the local time for the observations begins to vary from the nominal equatorial crossing times.

One solution to the diurnal sampling problem is to use numerical assimilation models. These models resample the satellite wind observations to regular (typically 6 hour) time intervals, and hence this would be the ideal place to bring diurnal information into the processing stream. This is further discussed in Section 5.

2.4 OW-CDR in the Pre-Satellite Era

While not detailed in this report, it is also worthwhile noting the potential of extending the OW-CDR back in time to before the satellite era (i.e. before 1987) using in situ observations. The wind speed calibration for the satellites described herein is nearly identical to that of visually estimated winds from Volunteer Observing Ships (VOS) (Li et al., 2015). The visual winds are based on the wind-driven sea state, which would be current relative, and related more directly to stress than to wind; implying that visual winds could have dependencies on atmospheric stability and currents similar to equivalent neutral winds. Li et al. (2015) suggested visual wind estimates can be used to extend a satellite-like wind climate record back in time, possibly as far back as 1900 in some areas, with the caveats that the VOS sampling is very different from satellite sampling and that the random uncertainty is close to 3 m/s.

3. Evaluating the OW-CDRs

3.1 Introduction

This section describes various means of evaluating the OW-CDRs. Each method has its advantages and limitations, as summarized here:

1. **Comparisons of OW retrievals with buoy winds**
   Plus: Provides absolute calibration for wind speed up to 15-20 m/s.
   Minus: Buoy data spatially very sparse; surface currents not available.
2. **Comparisons of OW retrievals with winds from numerical model (such as ECMWF and NCEP)**
   Plus: Global comparisons.
   Minus: Systematic errors exist in the numerical analyses and can be large.
3. **Comparisons of OW retrievals from sensors on two different platforms**
   Plus: Direct measurements of the same wind field; validation dataset not required.
   Minus: Comparisons limited by the required tight spatial/temporal collocation.
4. **Comparisons of OVW retrievals produced by different data providers**
   Plus: Reveals algorithmic uncertainties; validation data not required; no collocation issue.
   Minus: Does not reveal common system errors.

3.2 Wind CDR Accuracy Requirements

The World Meteorological Organization (WMO) Global Climate Observing System (GCOS) accuracy requirement on the OW-CDR is 0.5 m/s for low to moderate winds and 10% for winds exceeding 20 m/s (WMO, 2011). A stability requirement of 0.1 m/s/decade is also given. The GCOS temporal and spatial sampling requirements are 10 km and 3 hours. The 10-km resolution requirement is a compromise between a preferred scale of 5 km (or finer) and the reality that satellite sensor technology currently cannot achieve 5 km. A 5-km resolution is greatly preferred for near coastal applications, ocean and atmospheric applications involving curls and divergences, and for near-ice applications.

To meet the temporal requirement of 3 hours, the IOVWST recommended:

1. At least 3 sun-synchronous scatterometers in orbit.
2. One additional scatterometer in a non-sun-synchronous orbit (a) to determine the diurnal cycle of wind, (b) to provide better sampling at mid-latitudes, and (c) to improve sensor intercalibration.

These recommendations stem from the demonstrated usefulness of RapidScat observations of the diurnal and semi-diurnal cycle, and the benefits of closer and more plentiful collocations.

With respect to the GCOS stability requirement, the stability of the SSM/I sensors over 20 years was estimated to be 0.05 m/s/decade at the 95% confidence level (Wentz et al., 2007). More recently Wentz (2015) showed a relative stability of 0.03 m/s/decade among WindSat, QuikScat, and TMI over 10 years. Thus, it appears that the satellite sensors are meeting the GCOS stability accuracy requirement with a good deal of margin. This is fortunate because the OW-CDR record is now 3 decades, and the GCOS 0.1 m/s/decade requirement implies a 0.3 m/s drift error over 30 years is acceptable, when it most likely is not. The important role that buoys have to play in verifying long-term stability is discussed in the next subsection.

3.3 Buoy Wind Measurements Provide Absolute Calibration

Moored ocean buoys provide the absolute calibration reference for satellite wind retrievals. While the development of geophysical model functions (GMF) and wind retrieval algorithms rely on many inputs (numerical models, wind retrievals for other satellites, statistical constraints, etc.), the finalized satellite wind retrievals always need to be verified by comparisons with buoys. The buoy comparisons by themselves are not sufficient for complete validation, but they do provide a necessary constraint: when sufficiently averaged, the satellite winds need to agree with the buoys for winds below 15-20 m/s. If this condition is not met, then adjustments need to be made to the GMF/retrieval algorithm.

The moored buoy arrays most commonly used for validating satellite winds are the TAO/TRITON array in the tropical Pacific, the PIRATA array in the tropical and subtropical Atlantic Ocean, the RAMA array in the Indian Ocean, and the NDBC coastal buoys surrounding the United States (including Hawaii and Alaska). Other buoys are occasionally used, including the coastal buoys maintained by the Canadian Department of Fisheries and Oceans (although the quality control of these wind measurements is less stringent than that applied to the other buoy datasets).

When comparing satellite winds to buoy winds, one must account for

1) The different spatial and temporal sampling of buoy and satellites winds
2) The fact that radiometers and scatterometers are actually measuring surface roughness, not the wind.

Thus, concerning the latter, one should relate the buoy wind measurements to a surface stress value because it is generally assumed surface stress is the parameter most closely correlated with the surface roughness seen by the sensor. The surface stress is commonly expressed in terms of the 10-meter equivalent neutral wind (U_{10EN}). This conversion from buoy wind to surface stress must account for the buoy height, atmospheric stability, air density, and surface currents (Fairall et al., 1996, 2003; Plagge, 2012). At high winds, buoy measurements become less reliable (e.g., Zeng and Brown, 1998) and are typically excluded from the validation. For the operational buoy network, a high-wind limit of 15 m/s is often used. This limit is based on various buoy analyses (Large et al., 1995; Taylor and Yelland, 2001; Howden et al., 2008). However, with special adjustments for buoy roll and pitch and other factors, the high-wind limit could possibly be extended to 20 or 25 m/s (Edson et al, 2013).

Buoys are also useful for evaluating satellite winds in rainy areas. Detailed comparisons between collocated scatterometer and buoy vector winds have shown that ASCAT provides the most accurate wind speed and direction estimates in rain compared to buoy winds (Verspeek et al., 2010; Lin et al., 2012; Portabella et al., 2012; O'Neill et al., 2015). The reason is that ASCAT operates at C-band, which is less affected by radiative absorption and scattering than Ku-band sensors.

The accuracy of scatterometer winds in rain can have a surprisingly large impact on measured wind variance on time scales less than 5 days. There is a significant discrepancy between satellite and buoy estimates of temporal wind variability on time scales less than 5 days due to accuracy and sampling limitations of the satellite measurements, particularly those associated with rain accompanying ephemeral tropical convection. On timescales greater than 5 days, the scatterometer datasets provide good estimates of the lower frequency wind variability compared to the buoys, although the possibility exists that there could be small but important biases in rainy regions associated with systematic covariability of rain and wind in precipitating systems.

The need for the absolute wind calibration via ocean buoys will continue into the future. Satellite wind sensors are not perfectly stable, and small drifts in the 30-year OW-CDR observational record are an ongoing concern. In addition, when intercalibrating the numerous satellite sensors, there will be

small errors in the relative offsets that are applied. These offset errors will propagate like a random walk process, thereby introducing small spurious trends. These effects are expected to be small, as has been demonstrated by various analyzes of satellite data (see Section 3.2). However, keeping the spurious drift below 0.1 m/s over a 30-year span is challenging, and buoys are indispensable for validation.

This continuing need for buoy validation should be clearly communicated to the TPOS 2020 Project, which is currently assessing the future of the ocean buoy network in the tropical Pacific. The number and locations of buoys required for satellite validation need to be specified (Stoffelen and Vogelzang, 2015).

3.4 Numerical Model Winds Provide a Global Evaluation

Ocean vector winds calculated from today's numerical weather forecast models such as ECMWF, NCEP, and JMA provide an accurate representation of the near-surface ocean wind field. These wind fields are on regularly spaced temporal and spatial grids with no gaps. This grid structure greatly facilitates comparisons with orbiting satellite observations. The numerical models are useful for evaluating wind direction and a reference for wind speed evaluation, but with some caveats. Small systematic regional biases (≈0.5 m/s) between numerical model and satellite winds are typical and should be evaluated. The boundary layer physics governing the relationship between the near-surface winds reported by the model and the ocean surface stress measured by the satellites is regionally dependent and subject to some error (Sandu et al., 2013). In addition, because the quality, quantity, and type of assimilated datasets can change over time, long-term trends coming from numerical model reanalyses may be spurious. For long-term trends, one looks for decadal consistency among the various satellite sensors. Another caveat is that the models may not provide an accurate representation of winds in rainy areas and storms, where small-scale wind features like downdrafts are common.

Numerical model winds are useful for triple collocation analyses with buoy and satellite winds. Since validation datasets also have associated uncertainties, the best way to achieve an estimate of the confidence level for each wind product, satellite, buoy and model wind, is by using a triple-collocation technique (Stoffelen, 1998; McColl, 2014). This method compares, in pairs, three mutually-independent wind datasets collocated within a narrow time window. The root-mean-square error for each dataset is found by solving a simple set of three equations. This triple wind speed collocation method can also be applied for different wind speed regimes, to provide a confidence level as a function of wind speed.

3.5 Consistency in Winds from Sensors on Two Different Platforms

In constructing an OW-CDR, an essential requirement is that the OW from sensors on different satellites agree with each other when the two sensors are observing the same ocean area at the same time. Since exact space/time collocation is rarely achieved, a reasonable space/time collocation window is used. If this window is too large, then systematic diurnal variability and more random mesoscale variability will significantly contribute to real differences in the true vector wind fields. Ideally, spatial collocation windows of 25 - 50 km and temporal windows of about 1 hour are required. For sun-synchronous sensors, achieving a 1-hour collocation with another sensor can be a problem, as shown in Figure 3.5a. Also for convective storm systems, even a 1-hour collocation window will be too long (May and Bourassa, 2010).

A large time window up to 3 to 6 hours is unavoidable for some applications, and in these cases it must be recognized that the observed OW differences will contain a component that is not related to sensor/algorithm calibration problems. One possible way to mitigate the problems associated with large time windows is to do a long-term average (i.e., monthly) to reduce the error associated with

mesoscale variability. The remaining error due to systematic diurnal variability can possibly be accounted for using a diurnal model of OVW.

The preferred 1-hour collocation window is best achieved utilizing the satellite wind sensors that have inclined orbits like TMI, GMI, and RapidScat. The TMI/GMI combination now extends 19 years starting in 1998, and the RapidScat mission started in 2014. These inclined orbits rapidly precess through the diurnal cycle and provide 1-hour or even closer collocations every orbit with all operating sun-synchronous sensors. This approach to intercalibration is further discussed in Section 4.3.

Intercomparison of winds speeds from two sensors over many years provides an assessment of long-term stability. Figure 3.5b shows an example of this. In this figure, the RSS ASCAT-A wind speeds are compared to those from eight different satellite sensors. A large 4-hour collocation window is used, but this should not matter for assessing long-term stability as long as the globally averaged wind speed diurnal cycle does not vary in time. Relative to the other satellites, ASCAT appears to be very stable until late 2014, at which time there is a small negative shift (≈ -0.1 m/s) relative to all the other sensors, indicating that the shift can be attributed to an issue with ASCAT-A. EUMETSAT and KNMI have confirmed that ASCAT-A had some small issues with antenna calibration in the months of September-October 2014, and they are working to determine exact recalibration factors for each antenna.

Another example of comparing wind speeds from multiple sensors over an extended time period is given by Wentz (2015). This analysis uses 1-hour collocations of TMI retrieved wind speeds with 11 other satellite wind sensors. The longest intercomparison was TMI and WindSat, and this pair of sensors show a 0.02 m/s relative drift over the 12 years during which both sensors were in operation.

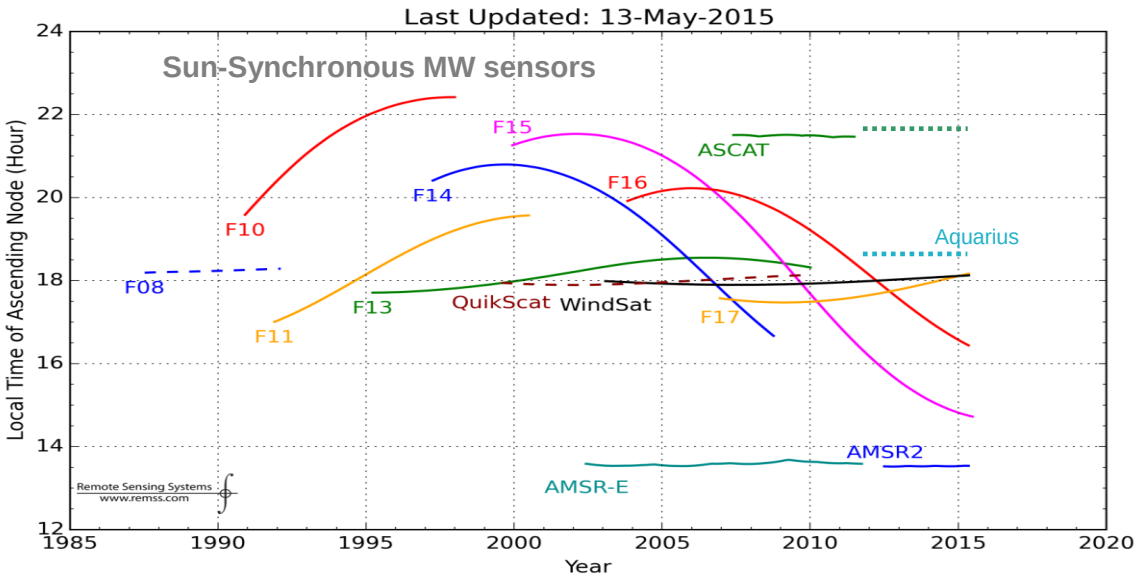

Figure 3.5a. Local time of the ascending node for the active and passive sun-synchronous wind observations, from 1988 until present (solid lines). QuikScat and F08 (dash lines) differ in that their descending node is plotted. Sensors with rapidly precessing orbits (TMI, GMI, and RapidScat) are not in the figure.

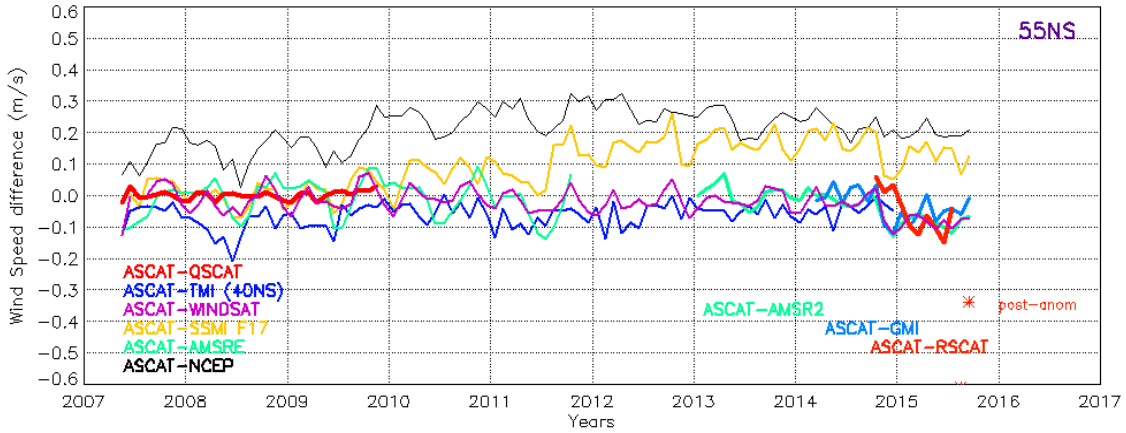

Figure 3.5b. Global monthly time series of the rain-free wind speed differences between the RSS ASCAT and the following sensors collocated to within 4 hours: QuikScat, TMI, WindSat, AMSRE, SSMI F17, AMSR2, GMI, and RapidScat. NCEP GDAS model winds are also compared. The red star at the end of 2015 represents the ASCAT-RapidScat bias during the post-anomaly state. Note that the F17 SSM/I has a known wind speed drift.

3.6 Intercomparison of OVW-CDR's from Different Institutions

3.6.1 Introduction

At the last OVWST Meeting, the Climate Working Group agreed to compare the OVW datasets produced by different institutions. By directly comparing OVW retrievals coming from different data providers, the systematic uncertainties due to the various retrieval methodologies and assumptions can be better understood. For this type of analysis, collocation is not a problem, and there is no need for ancillary validation datasets. The spatial and temporal sampling for the two datasets being compared will be the same. Intercomparison of CDRs from different institutions is a standard technique in climate research that has been used extensively in the IPCC Assessment Reports. Notably, the assessment of decadal changes in the Earth's tropospheric and stratospheric temperatures has relied on comparing results from three or four independent institutions (Karl et al., 2006; Thorne et al., 2011; Seidel et al., 2016).

This section describes the plan for doing an OVW Intercomparison Project. The objective is to quantify the differences in the various OVW datasets so that the uncertainties in the overall OVW retrieval process are better understood. This will hopefully lead to future improvements in OVW processing.

To limit the scope of the OVW Intercomparison Project to a manageable level, the project will begin by focusing on QuikScat and ASCAT-A. The full-swath QuikScat OVW record goes from 1999 to 2009, and the ASCAT-A observations started in 2007 and continue to the present. The two sensors now span 17 years and together provide the backbone for the OVW-CDR.

To further limit the scope of the first phase of the project, OVW retrievals in the presence of rain will be excluded to the extent possible. Ku-band OVW retrievals are significantly affected by rain and different retrieval algorithms handle the rain problem in different ways. Although C-band OVW retrievals are much less affected by rain, the accuracy of the numerical models, which are used for evaluation, is questionable in rainy areas. Excluding rain simplifies the analysis and allows us to focus on the more basic parts of the retrieval process.

3.6.2 Uniformity of Quality Control and Spatial/Temporal Gridding/Averaging

The first step is for the project participants to agree on a common set of data production criteria for conducting their analyses so that the results from the various institutions can be meaningfully examined. The production of OVW-CDRs is a complex process consisting of the following components:

1. Calculation of the sea-surface normalized radar cross section σ_o
2. Geophysical model function (GMF) that relates σ_o to vector wind, incidence angle, and frequency to first order and other parameters to second order
3. Vector wind retrieval algorithm and ambiguity removal algorithm
4. Quality Control (QC), including rain detection and exclusion
5. Spatial and temporal averaging and gridding

This OVW production can be divided into two parts: basic OVW retrieval (components 1-3) and post-processing (components 4-5). We note that QC is an essential part of the OVW retrieval process and could be included in the first part. However, for the first phase of the Intercomparison Project we want to isolate the effects of components 1-3 from the QC procedures. Each institution has their own methods for doing the first three steps, and it is this first part of the OVW processing we want to examine. To accomplish this, the project participants will agree on a common set of procedures for performing steps 4 and 5.

There is a close interplay among components 1-3. For example, biases in σ_o transfer to biases in the GMF such that σ_o – GMF is on the average equal to zero. Each data provider needs to describe, in detail, the methodology adopted for producing their dataset so that the OVW differences can be fully understood.

The choice of QC procedures can significantly affect intercomparison results. There are various QC algorithms currently in operation, and with some participant discussion, a consensus QC algorithm can hopefully be selected. The impact of QC on OVW can be better understood by performing comparisons for the same "QC regime". For example, results can be found for four different categories: when both datasets pass the QC, when both fail to pass the QC, and when one or the other passes QC. This stratification allows for a better understanding of the QC in each dataset and eventually leads to improvements/relaxation of rejecting thresholds in the QC algorithm.

3.6.3 Common Evaluation Metrics

Standard metrics include various statistical representation of the differences Δ_x in wind speed, wind direction, and the U and V wind components. For example, the mean and standard deviation of Δ_x can be stratified according to wind speed, SST, latitude, and swath position, and global maps of Δ_x can be made. Probability density functions of Δ_x are also a useful analysis tool.

Comparisons can be made on various spatial/temporal scales, ranging from instantaneous vector wind cells, to monthly or yearly 1^o latitude/longitude maps. A comparison of the curl and divergence fields from the different datasets would be particularly illuminating. The participants of the OVW Intercomparison Project will need to select a manageable number of analyses to perform.

3.6.4 Diurnal Cycle, Rain, and High Winds

QuikScat and ASCAT-A ascending node times are 6 am and 9:30 pm, respectively. The variability in ocean winds over the 3.5 hour difference can be large and tends to confound direct comparisons between QuikScat and ASCAT-A, particularly when doing precise analyses at the 0.1 m/s level. Mesoscale

variability in the wind field will produce significant random noise in the QuikScat-ASCAT differences and the diurnal cycle will produce systematic errors that will not go away with averaging. Each institution will need to deal with this time collocation problem in their preferred way, and this is expected to impact the QuikScat-ASCAT wind differences coming from the various institutions. For example, RapidScat and ASCAT 1-hour collocation can play a major role in the intercalibration of C- and Ku-band wind retrievals.

The first phase of the Intercomparison Project will exclude rainy observations to the extent possible because the interpretation of OVW retrievals in the presence of rain is complicated particularly for Ku-band measurements, which are more sensitive to radiative absorption and scattering than C-band measurements. Also, some Ku-band retrieval algorithms are designed to partially remove the influence of rain (Draper and Long, 2004; Fore et al., 2014) while others rely on an aggressive rain filter to exclude rainy observations (Ricciardulli and Wentz, 2014). In addition, the quality of the numerical model winds (like ECMWF and NCEP) in rainy areas is questionable. The impact of rain on the various OVW retrievals can be considered in a later phase of study.

There are several of ways that rain in a scatterometer footprint can be identified. First, rain imparts a discernible signature on the σ_o measurements that provides some information on rain contamination. Second, satellite microwave radiometers provide excellent estimates of rain, but to be useful these observations must be very close in time and space (30-60 minutes, 25 km) to the scatterometer observations. ASCAT on the MetOp missions could benefit from rain-estimates from the Microwave Humidity Sounder. Lin et al. (2014, 2015) have successfully used ASCAT estimates of wind variability (MLE and Singularity exponents) to identify areas of rain. These results suggest that it is the wind variability rather than the rain that affects the intercomparison. Two other useful microwave radiometers for rain-flagging are TMI and GMI, both operating in non-sun-synchronous orbits. TMI and GMI are therefore able to provide time collocations with the scatterometers at very short time scales, but for limited geographical regions. The CMORPH rain product also provides a useful ancillary dataset for identifying and excluding rain. A rain mask needs to be developed that can be used by all data providers to exclude OVW retrievals in rainy areas.

One area of major disagreement between methods used by different institutions is in the GMF calibration at high winds. At a recent High-Winds Workshop held in Miami in December 2015, significant progress was made towards establishing consensus on validation criteria for winds above 25 m/s. Although high winds are extremely important, they constitute a very small fraction of observations going into the construction of an OVW-CDR. In view of this, the OVW-CDR and the High-Winds Working Groups can proceed as fairly independent activities.

4. Extending the OW-CDRs into the Future

4.1 Introduction

A 30-year OWS-CDR consisting of 16 intercalibrated microwave imagers is currently available (Wentz,2013; Wentz 2015; Wentz and Draper 2016). The OWS-CDR is now being carried forward by nine operating radiometers: SSMI/SSMIS on DMSP platforms F15 through F19, WindSat, AMSR2, GMI, and SMAP. Of these, WindSat, AMSR2, and GMI are considered the most important.

A 16-year OVW-CDRs consisting of QuikScat (until the spin mechanism failure) and ASCAT-A is also available (Wentz and Ricciardulli, 2013; Stoffelen et al., 2015). More recently, RapidScat is being incorporated in the OVW-CDR, and ASCAT-B is being intercalibrated with ASCAT-A. These sensors, ASCAT-A, ASCAT-B and RapidScat, will carry the OVW-CDR forward in time, and in mid-2016 ScatSat will be added. Efforts are also underway to integrated the earlier ERS-1 and -2 scatterometers into the OVW-CDR.

In construction of both the OWS- and OVW-CDRs, an essential requirement is that the wind speeds from sensors on different satellites agree with each other when the two sensors are observing the same ocean area at the same time, as discussed in Section 3.5. For scatterometers operating at the same frequency (i.e., the Ku-band QuikScat, RapidScat, and ScatSat or the C-band ERS 1&2 and ASCAT A&B), the consistency in wind speeds is usually achieved by applying an offset to the σ_o measurements. The σ_o calibration offsets are determined by either (1) direct comparison of σ_o measurements from two collocated sensors or (2) by determining the σ_o offset that brings the wind speeds into agreement. For the first method, one must verify that the σ_o offset does indeed bring consistency to the wind speeds. Often a second residual adjustment, as discussed in Section 4.3, is needed to account for the non-linearities in the wind retrieval algorithm between σ_o and wind speed and other factors as well. It is generally the case that the σ_o offsets from the two methods are very similar. However, it must be realized that for the determination of an OW-CDR, consistency in both wind speed and σ_o is important.

Past experience has shown the benefit of utilizing both methods: direct σ_o intercalibration and wind speed intercalibration. These two methods are discussed in next two subsections.

4.2 Direct Intercalibration of Ku-band σ_o Measurements

Figure 4.2 shows a plan for producing a consistent set of Ku-band σ_o measurements starting with QuikScat in 1999 and continuing through to ScatSat to be launched in mid-2016. This intercalibrated 18-year time series of Ku-band σ_o measurements can then be used to produce an OVW-CDR. This method of directly intercalibrating the σ_o measurements (as opposed to intercalibrating wind speeds) has the advantage of providing global calibration information rather than being restricted just to the oceans. Vegetation and soil studies as well as ice research will certainly benefit from two decades of consistent Ku-band observations.

The original plan for the Ku-band σ_o intercalibration was to calibrate RapidScat to the non-spinning QuikScat, and then end the QuikScat mission and continue with just RapidScat. The inclined orbit of RapidScat (prograde 51.6^o inclination) will give 1-hour collocations with ScatSat every orbit. However, on August 14, 2015, RapidScat suffered a gain anomaly and went into a low signal-to-noise state. The impact of the gain anomaly is still unclear, but it certainly complicates the calibration procedure and brings into question the usefulness of RapidScat for the future calibration of ScatSat. In view of RapidScat's uncertain future, consideration is being given to continuing the QuikScat mission through 2016 and possibly into 2017. Under this option, both QuikScat and RapidScat would be available for calibrating ScatSat, and QuikScat would provide additional information on the RapidScat gain anomaly.

With respect to extending the QuikScat mission, a key consideration is the long-term stability of QuikScat. This question of stability is analyzed in the Appendix and is summarized here. The QuikScat instrument showed exceptional stability during its spinning phase: monitoring the rainforest shows a maximum instrument stability trend of -0.006 dB/year in normalized radar cross section (NRCS). The stability during normal operation was also demonstrated by comparing QuikScat wind speeds with TMI wind speeds. From 1999 to 2009, the relative drift of QuikScat minus TMI was only -0.025 m/s (Wentz, 2015).

After the instrument stopped spinning, no changes have been noticed in the instrument stability based upon onboard monitoring of observable parameters. The ability to provide calibration using the rainforest is somewhat degraded in the non-spinning state due to the narrow swath and fixed azimuth angles. Based upon the data observed over the Amazon, there is an intrinsic variability of 0.14 dB for 3-day averaging including both spatial-temporal variation in the natural target and instrument noise. The fit of the observed trends in σ_o constrain the maximum instrument term to be less than -0.02 dB/year. QuikScat remains the best calibration standard for direct calibration of backscatter cross-section at Ku-band. Based on these numbers, we estimate that calibration with ScatSat at better than 0.1 dB level could be done in less than a month. Achieving 0.05dB would require about 3 months. Given that the nominal ScatSat data availability starts in August 2016 (T. Misra, SAC-ISRO, private communication), static calibration using QuikScat could be achieved before QuikScat enters its eclipse phase in 2016. Monitoring ScatSat stability, should that instrument launch late or be unstable in its initial phase, would require operation of QuikScat after the 2016-2017 eclipse season.

The other important consideration for extending the Ku-band σ_o measurements is the current status of RapidScat. This is also analyzed in further detail in the Appendix, and the conclusions are given here. The ability of RapidScat to serve as a calibration platform was impacted by a hardware degradation that caused the instrument signal-to-noise to drop by about 10 dB. This drop has caused the winds estimated at speeds below 5 m/s to be impacted and require new calibration values, which are still being finalized. Nevertheless, for winds higher than 5 m/s and for bright rain forest targets, it is expected that the performance would not be impacted. Determining the stability of RapidScat at this point is premature, given that the time from the instrument degradation has been too short to determine a trend, and that instrument calibration using QuikScat is still ongoing. Nevertheless, we expect that the major contribution of RapidScat to OW CDR will be in its ability to serve as the tie point between observations occuring at different local times of day, where NWP models have proven insufficient. In addition, since RapidScat samples at exactly the same time as all other satellites in the constellation every revolution, it is an invaluable tool for determining regional differences in climate records between different instruments.

There are alternatives to a direct QuikScat/RapidScat/ScatSat Ku-band σ_o intercalibration. For ocean observations, the ScatSat σ_o calibration offsets can be obtained from the wind-speed intercalibration method discussed in the next subsection. Over land, the ScatSat σ_o calibration offsets can be based on stable land targets like the Amazon and Congo rainforests, as discussed in Section 4.4.

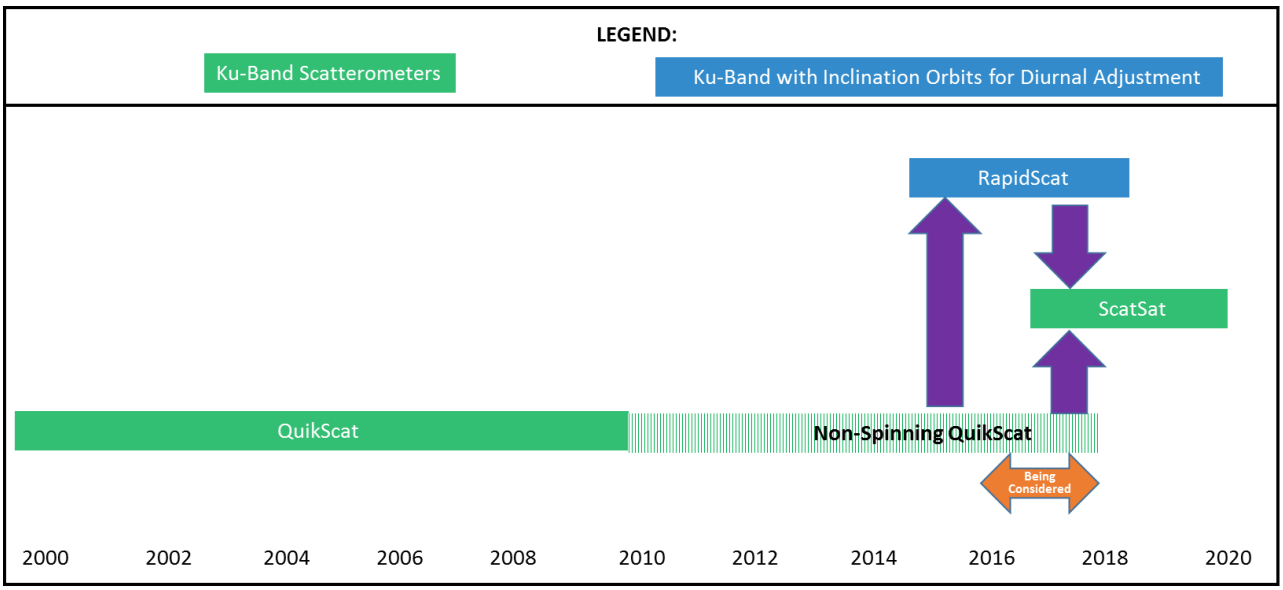

Figure 4.2. Direct intercalibration of Ku-band σ_o measurements.

4.3 Intercalibration of Wind Speed via Multiple Sensor Paths

One of the most demanding aspects of producing an OW-CDR is to achieve proper wind speed intercalibration over the large array of sensors that extend nearly 30 years. When ScatSat is launched in mid-2016, there will be about 12 other satellite wind sensors in orbit. For the most part, these 12 sensors will have been intercalibrated and can provide a very reliable wind speed reference for ScatSat.

Figure 4.3a shows the most reliable calibration paths that can connect the Ku-band ScatSat with the Ku-Band QuikScat. There are three paths shown in the figure:

1. QuikScat ➔ TMI ➔ ASCAT-A ➔GMI ➔ScatSat
2. QuikScat ➔ TMI ➔ WindSat ➔GMI ➔ScatSat
3. QuikScat ➔ TMI ➔ GMI ➔ScatSat

TMI and GMI are in low inclination orbits, and by using them as connecting sensors, 1-hour collocation windows can be obtained over the entire path. This avoids comparison of observations at different local times, and systematic errors related to the diurnal cycle are greatly mitigated. The local times for QuikScat and WindSat are 12 hours apart, and hence a 1-hour collocation window can be used over a good portion of the orbit (ascending orbit segment matching with a descending orbit segment). Thus, a fourth, more direct path can be used:

4. QuikScat ➔ WindSat ➔GMI ➔ScatSat

To assess the error in the wind speed intercalibration method using multiple sensors, Figure 4.3b shows global maps of the wind speed difference for ASCAT-A minus GMI and RapidScat minus WindSat. There are some interesting regional features reaching a magnitude of 0.5 m/s in some places. The cause of these differences is not fully understood, but their standard deviation (shown in Figure 4.3a) is small (0.1 to 0.2 m/s), and when averaged zonally, the regional differences are typically 0.2 m/s and do not exceed 0.3 m/s. For these results, observations in the presence of rain have been excluded using the rain flag provided by the collocated radiometer.

The first-order calibration of ScatSat requires applying a calibration offset to the σ_o measurements. Typically, one offset is applied to v-pol and another to h-pol. For the wind-speed calibration method discussed here, the offsets will be determined that remove the wind bias between ScatSat and other available wind sensors, (likely WindSat, GMI, AMSR2, ASCAT-A, and ASCAT-B). This calibration is done by globally averaging the wind speed differences. When globally averaged, the small regional differences shown in Figure 4.3b tend to zero.

A similar global wind calibration was done for RapidScat. In this case, the v-pol and h-pol σ_o calibration offsets were found by direct comparisons with the QuikScat measurements. Then, when the RapidScat winds coming from the RSS OVW algorithm were compared to WindSat, GMI, AMSR2, and ASCAT-A, a small negative offset of -0.21 m/s was found. Small wind offsets like this are to be expected considering the non-linearities in σ_o-to-vector wind algorithm, the particular choice of the GMF, details of the spatial sampling, and uncertainty in the QuikScat σ_o measurements use for calibration. The final step in the wind calibration was to remove the -0.21 m/s bias.

Table 4.3 shows the results of the RapidScat multi-sensor wind calibration. The RapidScat versus to WindSat, GMI, AMSR2, and ASCAT-A comparisons show remarkable similarity, with the four different wind offsets only varying by -0.03 to +0.05 m/s. This close agreement is indicative of the current state of the OWS-CDR.

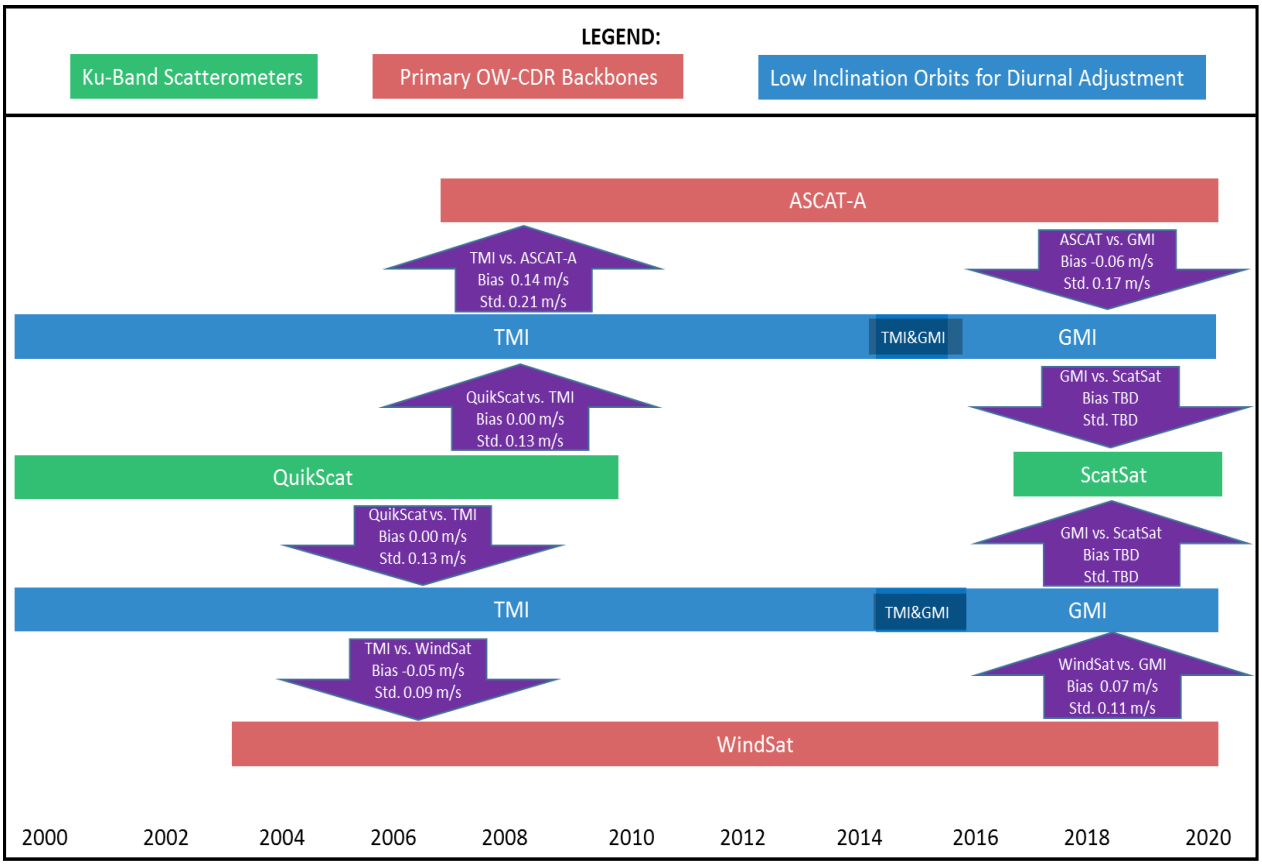

Figure 4.3a. Multiple paths for wind speed intercalibration. The bias and standard deviation are found by averaging over the pixels in the 1° latitude/longitude annual map of the wind speed difference.

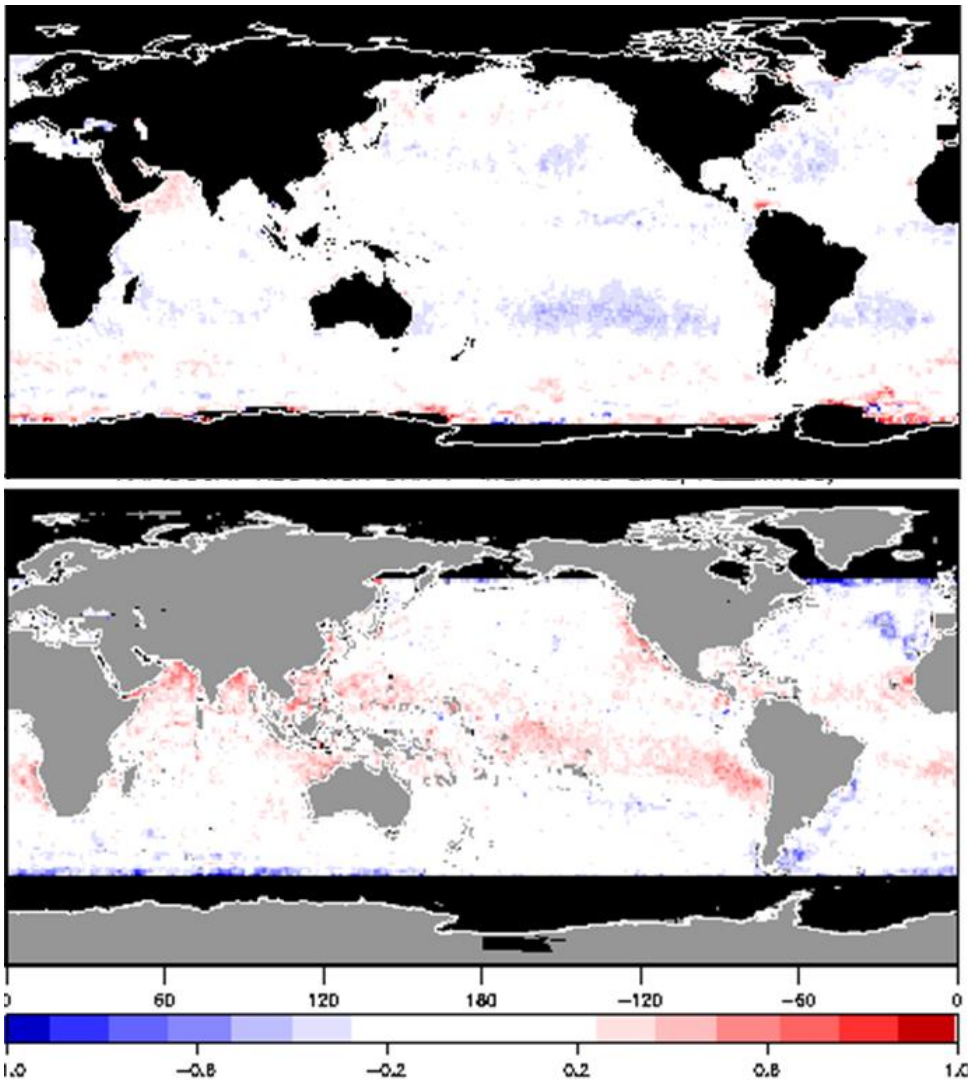

Figure 4.3b. Wind speed differences of ASCAT-A minus GMI (top panel) and RapidScat minus WindSat (bottom panel). The ASCAT-A/GMI results are a 2-year average (2014-2015), and the time collocation is 2 hours. The RapidScat/WindSat results are averaged from October 2014 to August 2015 (i.e., up until the RapidScat gain anomaly), and the time collocation window is 1.5 hours. Color scale is in units of m/s.

Looking at the various calibration paths, we see the importance of GMI in calibrating ScatSat. GMI flies in an inclined orbit (prograde 65° inclination) similar to RapidScat, and 1-hour collocations with ScatSat will be obtained every orbit. GMI has a dual on-board calibration system utilizing both external hot and cold loads and internal noise diodes. This advanced calibration system makes GMI arguably the most accurate satellite microwave radiometer to date (Wentz and Draper, 2016). The GMI observations extend from 65° S to 65° N, giving nearly complete coverage of the world's oceans. The GMI wind speed retrievals have been intercalibrated with other sensors and are now consistent with the existing OWS-CDR.

Previous analyses suggest that the σ_o calibration offsets found from the wind-speed calibration method are not necessarily applicable to land and ice observations. The reason for this is not clear, but this is one drawback to the wind speed calibration method. It may not provide sufficiently accurate σ_o calibration information over land and ice.

Table 4.3. Globally averaged wind speed difference of RapidScat versus 4 other satellite wind sensors. RapidScat winds are calibrated to agree with the average results obtained from the four comparison sensors.

Collocated Sensor Pair	Wind Speed Difference (m/s)
RapidScat-GMI	0.05
RapidScat-WindSat	-0.02
RapidScat-ASCAT-A	-0.03
RapidScat-AMSR2	-0.01

4.4 Rain Forest Calibration of ScatSat

Owing to their constant incidence angles and high degree of accuracy, pencil-beam scatterometer observations such as those from QuikScat, Oceansat-2 and RapidScat have also found use in various land applications. Most notably, the data have been used in sustaining the long record of sea-ice coverage (Remund and Long, 2014; Lindell and Long, 2016), studying drought conditions (Nghiem et. al, 2012), and identifying antecedent precipitation (Turk et. al., 2015). Each of these sensors employs dual beams at similar, but slightly different Earth incidence angles (EIA) and resolutions.

The brief Oceansat-2 and spinning QuikScat overlap period in November 2009 was used by Bhowmick et al. (2014) for cross-calibration, but a longer-term Ku-band radar reference is desirable to span the lifetimes of multiple sensors. Beginning in late 1997 with the launch of TRMM, continuous Ku-band surface backscatter observations have been collected by the NASA/JAXA Precipitation Radar (science operations ended in late 2014), and the GPM Dual-Frequency Precipitation Radar (DPR) (March 2014-current), giving an approximate 9-month overlap period. Since the time record covers all scatterometer missions mentioned above, these observations could potentially serve as a source for long-term cross-referencing between individual scatterometer sensors.

The variability in the multispectral σ_o (including TRMM/PR) over several land surface types was studied by Stephen and Long (2002). For scatterometer cross-calibration, a complication arises since both the PR and DPR radars scan an approximate 240-km swath at 49 incidence angles between $\pm 17^o$ degrees about nadir, unlike the viewing angle range of the scatterometers mentioned above which fall between the range of 45^o and 55^o. Over most land surfaces, the high variability of the near-nadir backscatter (Meneghini and Jones, 2011) limits the utility of these data for cross-referencing. The exception is for dense-enough vegetation, such as that found in the rainforests in the Amazon, the Congo and other self-similar locations, where the backscatter is fairly constant past $10^o - 15^o$ from nadir. This behavior is illustrated in Figure 4.4a, which contrasts the off-nadir Ku-band σ_o variability for bare soil and heavy vegetation, using the Durden et al. (2012) classification. The variability in vegetation is even less in specific regions, notably tropical rain forests.

RapidScat is now providing a precise characterization of the diurnal variation of radar backscatter over land. By nature of its non-synchronous orbit, RapidScat is the first scatterometer capable of observing σ_o over the full 24-hour cycle (Paget et al., 2016). In addition, RapidScat has enabled improved cross-calibration between scatterometers operating at different local-times-of-day, e.g., Madsen and Long (2016).

To illustrate, the top panel of Figure 4.4b shows the time series from 1998 to late 2015. In this figure, each point represents the Ku-band σ_o nearest to a location in the Amazon (the PR resolution is ≈4-km, so a 3x3 region is averaged to approximate the scatterometer footprint-level σ_o resolution), from the start of PR and into the GPM era (with the limited swath, the observations occurring once every 3-4 days). The mean is near ≈ -6 dB, with about ±1 dB variability, across all 17 years. The bottom panel

shows the corresponding inner and outer-beam observations from QuikScat, Oceansat-2, and RapidScat, during each respective operating period. For each, the mean value is about 3 dB smaller, and the natural variability is slightly larger than noted for PR/DPR. This suggests that despite these observational differences, the long record of PR/DPR observations over dense vegetation are useful for identifying unexpected changes to instrument operating characteristics. For example, the period in early 2010 when the OceanSat-2 σ_o dropped by about 0.5 to 1 dB is noted, whereas the same fluctuations are not noted in the PR σ_o, suggesting that the change may be OceanSat-2-related. Indeed, this change in OceanSat-2 σ_o was related to a known 0.5 dB power drop in OceansSat-2 in August 2010 (Jaruwatanadilok et. al., 2013). The bottom panels of Figure 4.4b show these same plots, but over a region in the Congo (0.47N 21.57E). Similar range in σ_o variability is observed, but the mean of each time series is shifted slightly (PR is slightly lower than was noted in the Amazon, whereas the scatterometer σ_o is slightly higher), owing to the different vegetation characteristics. This suggests the utility of the long-term record of Ku-band σ_o in the 12-17 degree range, that continues today with GPM/DPR, for calibrating the ScatSat σ_o records over land, with due consideration for the diurnal cycle.

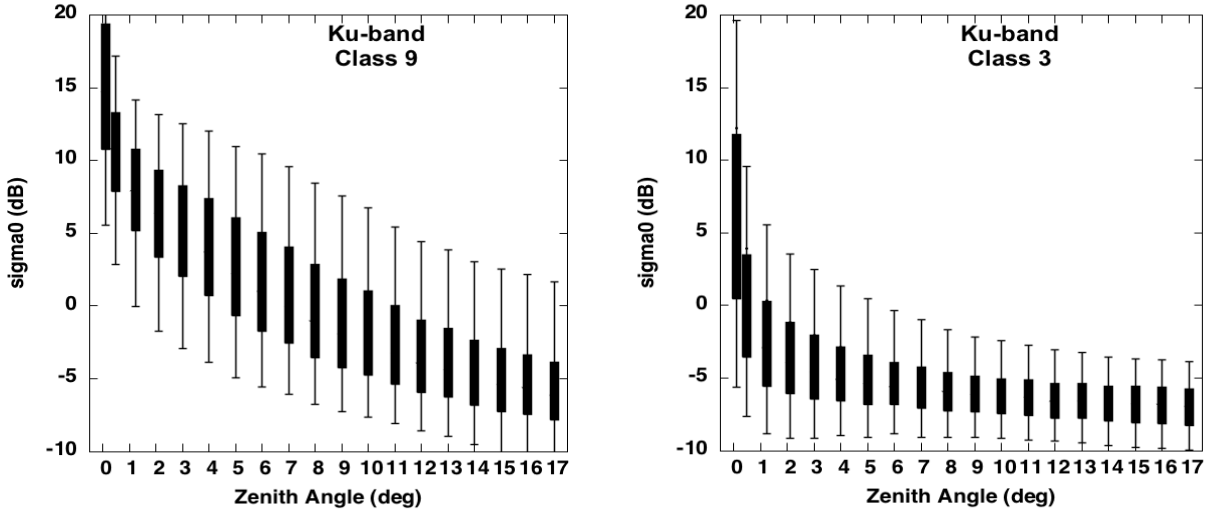

Figure 4.4a. Box-and-whisker figures illustrating the variability (5, 25, 75 and 95 percent quartile) of the Ku-band DPR backscatter over bare soil (left) and dense vegetation (right) at incidence angles up to 17-degrees from nadir, using the Durden et. al. (2012) classification.

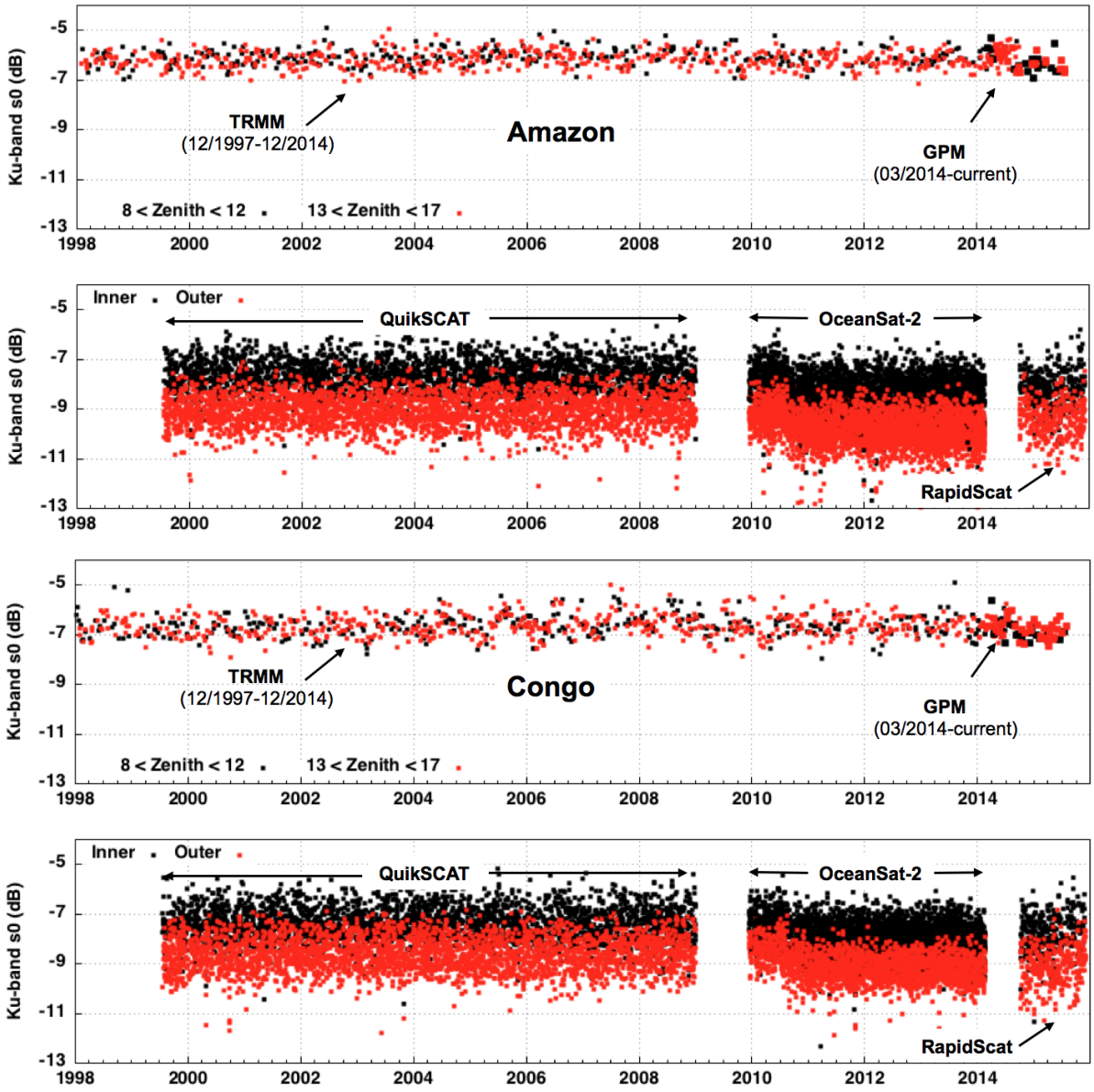

Figure 4.4b. (Top) Time series from 1998 to late 2015 for TRMM Precipitation Radar and GPM Dual-Frequency Precipitation Radar surface backscatter cross section, and the individual periods of record for each of QuikScat, OceanSat-2, and RapidScat, for a location in the Amazon (2.41S 63.15W). (Bottom) Same as top panels, but for a location in the Congo (0.47N 21.57E).

4.5 Summary

This section has discussed various methods and strategies for extending the OW-CDRs into the future, with particular focus on incorporating ScatSat into the OW-CDR. Table 4.5 summarized the various options. By exploiting all options, multiple consistency checks can be done that will lead to a well-verified OW-CDR.

There are plans in place to use all of these calibration methods, with the possible exception of QuikScat. QuikScat will add value to the OW-CDR calibration process. In addition, QuikScat provides

the means to continue the time series of Ku-band σ_o measurements over land and ice. However, this requires extending the QuikScat mission through 2016 and possibly into 2017.

RapidScat is the only vector wind sensor that views the ocean throughout the complete 24-hour cycle. This unique capability has great potential for (1) cross-calibrating sun-synchronous sensors and (2) characterizing the diurnal variability of winds over the world's oceans. While there are other methods for cross-calibrating sun-synchronous sensors, there is no substitute for the diurnal wind information coming from RapidScat. It is too soon to understand the full implications of RapidScat's gain anomaly. However, given the unique diurnal capabilities of this sensor, effort should be directed towards overcoming the gain anomaly and extracting as much information as possible from this sensor.

Table 4.5 Calibration Methods for Extending the OW-CDR into the Future

Calibration	Advantages	Limitations
QuikScat	- Measures σ_0 at same incidence and polarization - Has proven long-term stability - σ_0 calibration independent of geophysical model function - Calibration within 0.1dB in one month	- one azimuth angle and narrow swath - Requires 3 months averaging for 0.05 dB calibration, 6 months to observe trends - Does not sample at the same time - Wind retrievals not possible without independent direction information
RapidScat	- Provides measurements simultaneous in time - Provides wide swath Ku-band winds - Rainforest calibration unaffected by low SNR state: can monitor Amazon drift - Provides a direct way of cross-calibrating sun-synchronous satellites - ISS availability through summer 2017	- Low SNR state has unknown long-term stability - Current stability estimates will require multiple months for calibration - Not officially funded through late summer 2017
ASCAT	- Proven stability and known wind performance - Local times similar to ScatSat during ScatSat early phase	- Cannot provide direct σ_0 stability assessment over land and ice - Assessment sensitive to GMF limitations and changes - Small regional differences exist between the C and Ku band winds
Radiometers	- Availability of long-term wind speed CDR among many different platforms - Diversity of local times - Consistency among sensors better than 0.1 m/s - Several sensors available for ScatSat calibration (GMI, WindSat, AMSR2)	- Cannot provide direct σ_0 stability assessment over land and ice - Assessment sensitive to GMF limitations and changes - Cannot be used to validate directions or derivatives
Land Calibration	- Provides long-term continuity between instruments - Average variability is small	- Provides a drift reference, but not absolute calibration - Could vary in the near term due to El Niño induced drought
NWP Model	- Consistent wind reference for multiple platforms	- Long term biases can be introduced as data being ingested or methodology changes - Cannot resolve with sufficient resolution to validate divergence or curl - NWP models have distorted representation of the diurnal signal

5. Specialized Model Assimilation of Satellite Winds

5.1 Motivation

The objective of specialize model assimilations is to provide vectors winds on a regularly spaced temporal/spatial grid while preserving the satellite wind information. These specialized assimilations offer the prospect of mitigating the long-standing problem of constructing a composite OW-CDR from multiple satellites viewing the Earth at different local times. In contrast, much of the satellite wind information is lost in large general-purpose numerical weather forecast models like ECMWF and NCEP. Specialized assimilations fill the gap between single satellite products and the numerical weather forecast models. These Earth gridded vector winds greatly facilitate many science and operational applications

Since the assimilation models resample the satellite wind observations to regular (typically 6 hour) time intervals, and this would be the ideal place to bring diurnal information into the processing stream. However, this will require a better understanding of the diurnal variations of winds over the world's oceans. In this regard, RapidScat is indispensable. RapidScat is the only scatterometer that views the ocean at all times of the day. The radiometers TMI and GMI provide diurnal wind speed information, which is certainly helpful, but much of the diurnal signal is characterized in terms of the U and V components of the wind field.

We face three main challenges in directly using wind observations from satellites for understanding and predicting the atmosphere and ocean:

1. Incomplete spatial and temporal sampling of the transient and evolving wind field. Several authors, most recently Patoux and Levy (2013), have shown that using satellite data alone allows only a horizontally coarse analysis at time intervals that cannot resolve the diurnal cycle. Moreover, the temporal sampling is much coarser than the atmospheric time scale of evolution of these scales.
2. Data dropouts due to precipitation in moist convective regions. The latter are reduced at lower operating frequency, e.g., ASCAT vs. QuikScat; and
3. Many of the satellite sensors only provide wind speed, not direction.

With respect to numerical weather prediction (NWP) data assimilation (DA) products, these provide complete coverage of wind speed and direction, but generally lack deterministic mesoscale structure.

5.2 Advantages of specialized assimilations for OVW

The advantages of specialized assimilations for OVW include the following.

1. Specialized assimilations can take advantage of the full volume of microwave active and passive ocean winds, whereas only a small fraction is typically used in NWP assimilation systems.
2. Specialized assimilations can provide analyses on the smallest possible space and time scales. For example, CCMP (described below) provides analyses every 6 hour with 25-km grid spacing over the world oceans. Another example is the Centre for Earth Observation Satellites, which coordinates an Ocean Surface Vector Winds Virtual Constellation (OSVW VC) to improve spatial-temporal coverage (ceos.org/ourwork/virtual-constellations/osvw/).

3. Specialized assimilations can represent processes and detect new circulations and features not present in NWP fields. Also essential dynamical aspects of the air-sea ocean interface that may be included in specialized assimilations such as ERA* described below due to the additional information from satellite winds include:

    a. Ocean eddy scale dynamics
    b. Air-sea interaction near moist convection
    c. Wind direction correction in stable atmospheric flow (Sandu et al., 2013)

4. As a by-product, specialized assimilations can be used to assign directions to wind speed only data.

5. Specialized assimilations can be designed to provide consistent sets of wind stress and other fluxes.

5.3 Limitations of specialized assimilations for OVW

The main limitation of specialized assimilations for OVW is inhomogeneous sampling. There are regions and times where there are no satellite observations. There are also rain dropouts in the data swath. In many blended products, in case of no observations, a background field is used to fill in the data. For rain dropouts, moist convection is generally poorly represented in global NWP (Lin et al., 2015). In ERA* (described below) homogeneous sampling is achieved by computing local mean and variable adaptations to ERA over a few days, therefore, the product characteristics are spatially more uniform. While not really a limitation, it must be recognized that satellite winds are relative to ocean currents rather than relative to a fixed Earth surface.

Another limitation of the use of specialized assimilations is the difficulty of maintaining the subtle decadal wind trends that are contained in the satellite observations. These trends can be small (0.1 m/s/decade) and can be distorted by the background field and by resampling. As one remedy, the satellite record can be used to monitor and correct for these types of systematic errors.

5.4 Technical approach

In general, data assimilation methods seek the minimum of an objective function that measures the misfits of the analysis to observations, background, and constraints. This can also be true for specialized assimilations of OVW, including most examples listed below. Methods differ in the details of the definition of the observation, background, and constraint functions, in what data are used, in the QC procedures that are applied, and in the solution method. Input data types may be radiances, backscatter measurements, retrieved winds speeds and/or retrieved wind directions. Retrieved quantities include some information from prior information used in the retrieval. This is accounted for in the analysis method, usually by tuning the weight given to these data. For OVW the QC usually eliminates observations affected by enhanced wind variability, precipitation and land and ice contamination. Typically, the solution method to find the minimizing analysis is based on the conjugate gradient approach.

5.5 CCMP

The cross-calibrated multiplatform (CCMP) is one example of a long-term high-resolution accurate specialized assimilation of OVW (Atlas et al. 2011). CCMP is based on a proven, efficient variational analysis method (VAM) that is particularly well suited to the blending of different sources of ocean surface wind information in order to determine accurate high-resolution (spatial and temporal) vector wind fields (Atlas et al. 2011). Note that the VAM analysis of satellite surface wind data adds small-

scale variability to the ECMWF background (Atlas et al. 2011, Fig. SB1), when sampled. Since much of the data used in CCMP processing are wind speeds from microwave radiometers, the VAM analyzed vector wind fields are used to assign directions to satellite wind speed observations. For the CCMP OVWs, the input satellite data are the RSS cross-calibrated wind speeds derived from SSMI/SSMIS, TMI/GMI, AMSRE/AMSR2, and WindSat and wind vectors are from QuikScat. All these satellite winds are combined with conventional ship and buoy data and ECMWF reanalyses or operational analyses by the VAM.

The CCMP OVWs (v1.1) for the period 1987 to 2011 are a community resource available through JPL's Physical Oceanography data archive (http://podaac.jpl.nasa.gov/Cross-Calibrated_Multi-Platform_OceanSurfaceWindVectorAnalyses). There are over 100 known references to work using CCMP OVWs in the refereed literature. CCMP v2.0 was recently released by RSS in January 2016. This re-processing and update of CCMP uses the most current and complete RSS cross-calibrated wind datasets - including ASCAT, uses the ECMWF Interim reanalysis as a consistent and higher resolution background, and extends the data period to the present. See:
http://www.remss.com/measurements/ccmp

5.6 ERA*

Many users use the ECMWF Reanalysis (ERA) (Dee et al., 2011) as a convenient and consistent dynamical record of the atmosphere over the recent decades. ERA provides gridded fields every 3 hours (forecasts) or 6 hours (analyses). However, high-quality mesoscale wind observations, such as those from scatterometers and radiometers are rather poorly exploited. Spatial resolution is limited to a few 100 km over the open ocean due to its 80-km grid and dynamical closure (e.g., Vogelzang et al., 2011). Therefore, essential dynamical aspects of the air-sea ocean may be added by using satellite winds.

In ERA* (Stoffelen et al., 2015) these aspects are being added after evaluation of their systematic and variable impact with respect to ERA. To this end, differences between satellite observations and collocated ERA are computed and locally their mean and SD are stored. The systematic effects and variances appear rather similar from day to day and depict the above effects, which generally evolve slowly locally in terms of their mean and SD. The variance is mainly caused by moist convection and dominates in the tropical moist convection regions, where its associated sea surface wind variability dominates the air-sea interaction (Lin et al., 2015). The first year of ERA* will be ASCAT and QuikScat will then follow to test the effects of the diurnal cycle.

To produce ERA*, the evolving mean differences are easily applied as corrections to all ERA-interim stress-equivalent wind or derivative fields and thus constitute an improved representation of the abovementioned phenomena in ERA. Further perturbations to ERA are probably meaningful to represent the variance of the difference, constituting wind variability in convection areas. It is, in particular, this wind variability that is generally ignored, or worse, removed as noise, in other blended wind and stress products. ERA* is being verified against buoy winds and tested in ocean modeling (Stoffelen et al., 2015). Note that ERA* uses archived reanalysis backgrounds and is provided 3-hourly.

5.7 Approaches under development and suggestions for improvement

There is a middle ground between producing a regularly gridded field through purely statistical data assimilation and through an NWP reanalysis. The statistical methods can assimilate NWP products (e.g., the OAFLUX product) and it can include a constraint on the nearness of fit to reanalyses (e.g., the CCMP product); however, neither of these approaches makes the resulting product consistent with the physical relationships imposed in the NWP assimilation.

One such middle ground is a statistical approach that includes several of these physical constraints as hard constraints, or highly weighted soft constraints. Such an approach is being developed at FSU. One difficulty is that the link between the surface winds, Ekman winds, and geostrophic winds should apply globally. Models of such constraints have not applied well in both the tropics and the mid-latitudes (e.g., the University of Washington Planetary Boundary-Layer Model). A new constraint, based on the framework of Stommel (1953) was extended to include all these layers. It has been modified to allow non-uniform zonal wind stress and non-zero temperature fronts, and has been shown to work in the tropics (as per Bonjean & Lagerloef (2002)) and mid-latitudes (albeit currently as a rather time consuming calculation). Nevertheless, this constraint can be applied to produce a smoother field that continues to include realistic features and much finer resolution than the statistical assimilation. Preliminary results have shown that this type of approach can roughly reproduce the observed dependence of spatial variability in wind as a function of the SST gradient. Such relationships are not found in NWP or in purely statistical products, except in a greatly weakened form. This dependency has been found without forcing it explicitly, but rather due to the dynamics imposed by the hard constraint. This middle approach is a promising alternative to more traditional approaches to producing regularly gridded fields.

Potential enhancements of specialized assimilations for OVW include the following.

- *Use of archived reanalysis backgrounds*. Note that modern NWP DA systems assimilate some of the in situ and satellite ocean winds that might be used in a specialized assimilation. In the future, it would be desirable to use archived reanalysis backgrounds (3, 6, 9 h forecasts) to avoid the potential double use of some of the observations. This would also allow a specialized assimilation with 3 h temporal resolution.
- *Use of additional data sources*. Data from OceanSat-2, RapidSCAT, CYGNSS, and other future sensors might be included in specialized assimilations.
- *Provide enhanced uncertainty estimates*. Specialized assimilations should provide validated uncertainty estimates for each analysis quantity.
- *Assimilation of non-wind variables, such as surface temperature gradients and surface pressure*.

.

6. References

Atlas, R.M., R.N. Hoffman, J. Ardizzone, S.M. Leidner, J.C. Jusem, D.K. Smith, and D. Gombos, 2011: A cross-calibrated, multi-platform ocean surface wind velocity product for meteorological and oceanographic applications. *Bulletin of the American Meteorological Society, 92*, 157-174.

Bhowmick, S.A., R. Kumar, and A.S.K. Kumar, 2014: Cross calibration of the OceanSAT-2 scatterometer with QuikSCAT scatterometer using natural terrestrial targets. *IEEE Transactions on Geoscience and Remote Sensing, 52*, 3393-3398.

Bonjean, F. and G.S. Lagerloef, 2002: Diagnostic model and analysis of the surface currents in the tropical Pacific Ocean. *Journal of Physical Oceanography,* 32**,** 2938–2954.

Dee, D.P., and Coauthors, 2011: The ERA-Interim reanalysis: Configuration and performance of the data assimilation system. *Quarterly Journal of the Royal Meteorological Society, 137*, 553-597.

Draper and D.G. Long, D.W., 2004: Simultaneous Wind and rain retrieval using SeaWinds data. *IEEE Transactions on Geoscience and Remote Sensing, 42*, 411-1423, doi:10.1109/TGRS.2004.830169.

Durden, S.L., S. Tanelli, and R. Meneghini, 2012: Using surface classification to improve surface reference technique performance over land. *Indian Journal of Radio & Space Physics 41*, 403-410.

Edson, J.B., and Coauthors, 2013: On the exchange of momentum over the open ocean. *Journal of Physical Oceanography*, 43, 1589–1610.

Fairall, C.W., G.S. Young, E.F. Bradley, D.P. Rogers, and J.B. Edson, 1996: Bulk parameterization of air-sea fluxes for Tropical Ocean-Global Atmosphere Coupled-Ocean Atmosphere Response Experiment. *Journal of Geophysical Research, 101*, 3747-3764.

Fairall, C.W., E.F. Bradley, J.E. Hare, A.A. Grachev, and J.B. Edson, 2003: Bulk parameterization of air–sea fluxes: Updates and verification for the COARE algorithm. *Journal of Climate, 16*, 571–591.

Fore, A.G., B.W. Stiles, A.H. Chau, B.A. Williams, R.S. Dunbar, and E. Rodriguez, 2014: Point-wise wind retrieval and ambiguity removal improvements for the QuikSCAT climatological data set. *IEEE Transactions on Geoscience and Remote Sensing, 52,* doi:10.1109/TGRS.2012. 2235843.

Gille, S. T., 2005: Statistical Characterization of Zonal and Meridional Ocean Wind Stress. *Journal of Atmospheric and Oceanic Technology, 22*, 1353-1372.

Gille, S. T., S. G. L. Smith and S. M. Lee, 2003: Measuring the Sea Breeze from QuikSCAT scatterometry. *Geophysical Research Letters, 30*(3), 1114, doi:10.1029/2002GL016230.

Howden, S., D. Gilhousen, N. Guinasso, J. Walpert, M. Sturgeon, and L. Bender, 2008: Hurricane Katrina winds measured by a buoy-mounted sonic anemometer. *Journal of Atmospheric and Oceanic Technology, 25*, 607-616.

Jaruwatanadilok, S., B.W. Stiles, and A.G. Fore, 2013: Cross-calibration between QuikSCAT and Oceansat-2. *IEEE Transactions on Geoscience and Remote Sensing*, *52*, 6197-6204.

Karl, T. R., S. J. Hassol, C. D. Miller, and W. L. Murray, 2006: Temperature trends in the lower atmosphere: Steps for understanding and reconciling differences, U.S. Climate Change Science Program and the Subcommittee on Global Change Research Final Report Rep., Washington D. C.

Large, W. G., J. Morzel, and G. B. Crawford, 1995: Accounting for surface wave distortion of the marine wind profile in low-level ocean storms wind measurements. *Journal of Physical Oceanography, 25*,

2959-2971.

Li, K., M. A. Bourassa, and S. R. Smith, 2015: Adjustment of visually observed ship winds (Beaufort winds) in ICOADS. Poster presented at 2015 International Ocean Vector Winds Science Team Meeting, 19-21 May 2015, Portland, OR.

Lin, W., M. Portabella, A. Stoffelen, and A. Verhoef, 2012: On the characteristics of ASCAT wind direction ambiguities. Atmospheric Measurement Techniques Discussions, 5, 8839-8857.

Lin, W., M. Portabella, A. Stoffelen, A. Turiel, and A. Verhoef, 2014: Rain identification in ASCAT winds using singularity analysis. *IEEE Geoscience and Remote Sensing Letters, 11,* 1519-1523.

Lin, W., M. Portabella, A. Stoffelen, A. Verhoef, and A. Turiel, 2015: ASCAT wind quality control near rain. *IEEE Transactions on Geoscience and Remote Sensing, 53*, 4165-4177.

Lindell, D.B., and D.G. Long, 2016: Multiyear arctic sea ice classification using OSCAT and QuikSCAT. *IEEE Transactions on Geoscience and Remote Sensing*, 54, 167-175, doi:10.1109/TGARS.2015.2452215.

Madsen, N. M., and D.G. Long, 2016: Calibration and Validation of the RapidScat Scatterometer Using Tropical Rainforests. *IEEE Transactions on Geoscience and Remote Sensing*, to appear, doi:10.1109/TGARS.2015.2506463.

May, J., and M. A. Bourassa, 2011: Quantifying variance due to temporal and spatial difference between ship and satellite winds. *Journal of Geophysical Research*, 116, DOI:10.1029/2010JC006931.

Meneghini, R., and J.A. Jones, 2011: Standard deviation of spatially averaged surface cross section data from the TRMM Precipitation Radar. *IEEE Geoscience and Remote Sensing Letters*, *8,* 293-297.

McColl, K.A., J. Vogelzang, A.G. Konings, D. Entekhabi, M. Piles, and A. Stoffelen, 2014: Extended triple collocation: Estimating errors and correlation coefficients with respect to an unknown target. *Geophysical Research Letters, 41*, 6229–6236, doi:10.1002/2014GL061322.

Nghiem, S., B.D. Wardlow, D. Allured, M.D. Svoboda, D. LeComte, M. Rosencrans, S. Chan, and G. Neumann, 2012: Microwave remote sensing of soil moisture: Science and applications. In *Microwave Remote Sensing of Drought: Innovative Monitoring Approaches* (Boca Raton, FL: CRC Press).

O'Neill, L. W., T. Haack, and T. Durland, 2015: Estimation of time-averaged surface divergence and vorticity from satellite ocean vector winds. *Journal of Climate, 28*, 7596-7620.

Paget, A.P., D.G. Long, and N.M. Madsen, 2016: RapidScat diurnal cycles over land. *IEEE Transactions on Geoscience and Remote Sensing*, to appear, doi:10.1109/TGRS.2016.2515022.

Patoux, J., and G. Levy, 2013: Space-time interpolation of satellite winds in the tropics. *Journal of Geophysical Research Atmospheres, 118*, 10,405–10,413, doi:10.1002/jgrd.50811.

Plagge, A. M., D. Vandemark and B. Chapron, 2012: Examining the impact of surface currents on satellite scatterometer and altimeter ocean winds. *Journal of Atmospheric and. Oceanic Technology, 29*, 1776-1793, 2012, doi: http://dx.doi.org/10.1175/JTECH-D-12-00017.1.

Portabella, M., A. Stoffelen, W. Lin, A. Turiel, A. Verhoef, J. Verspeek, and J. Ballabrera-Poy, 2012: Rain effects on ASCAT-retrieved winds: Toward an improved quality control. *IEEE Transactions on Geoscience and Remote Sensing, 50*, 2495-2506.

Remund, Q.D. and D.G. Long, 2014: A decade of QuikSCAT scatterometer sea ice extent data. *IEEE Transactions on Geoscience and Remote Sensing*, doi:10.1109/TGRS.2013.2281056, *52*(7), 4281-4290.

Ricciardulli, L, and F. Wentz, 2014: "Progress and future plans on an ocean vector wind climate record", presented at the International Ocean Vector Wind Science Team meeting, Brest, France, June 2014. Available at https://mdc.coaps.fsu.edu/scatterometry/meeting/docs/2014/ClimateDataRecord/Ricciardulli_ovwst_2014_CDR_posted.pdf

Ricciardulli, L. and F.J. Wentz, 2015: A scatterometer geophysical model function for climate-quality winds: QuikSCAT Ku-2011. *Journal of Atmospheric and Oceanic Technology, 32*, 1829–1846.

Sandu, I., A. Beljaars, P. Bechtold, T. Mauritsen, G. Balsamo, 2013: Why is it so difficult to represent stably stratified conditions in numerical weather prediction (NWP) models? *Journal of Advances in Modeling Earth Systems, 5*, 117–133, doi:10.1002/jame.20013.

Seidel, D. J., J. Li, C. Mears, I. Moradi, J. Nash, W. J. Randel, R. Saunders, D. W. J. Thompson, and C.-Z. Zou, 2016: Stratospheric temperature changes during the satellite era, *Journal of Geophysical Research,* to appear, doi: 10.1002/2015JD024039.

Stephen, H., and D.G. Long, 2002: Multi-spectral analysis of the Amazon basin using SeaWinds, ERS, Seasat scatterometers, TRMM-PR and SSM/I. *2002 IEEE International Geoscience and Remote Sensing Symposium, IGARSS '02*, (Volume:3), 1780-1782.

Stoffelen, A., 1998: Toward the true near-surface wind speed: Error modeling and calibration using triple collocation. *Journal of Geophysical Research, 103*, 7755-7766.

Stoffelen, A., A. Verhoef, J. de Kloe, and Coauthors, 2015: Scatterometer Stress-Equivalent Winds for Ocean and Climate Applications. EUMETSAT User Conference, Toulouse, France, Sept. 2015, available online from Stoffelen.pdf located in http://www.eumetsat.int/website/wcm/idc/idcplg?IdcService=GET_FILE&dDocName=ZIP_CONF_2015_S4_ORAL&RevisionSelectionMethod=LatestReleased&Rendition=Web

Stoffelen, A., and J. Vogelzang, 2015: On buoys, scatterometers and reanalyses for globally representative winds, KNMI Document NWPSAF-KN-TR-024. https://nwpsaf.eu/deliverables/scatterometer/reports/nwpsaf-kn-tr-024.pdf

Stommel, H. 1953: Wind-drift near the equator. *Deep Sea Research,* 6**,** 298–302.

Taylor, P. K., and M. J. Yelland, 2001: Comments on "On the Effect of Ocean Waves on the Kinetic Energy Balance and Consequences for the Inertial Dissipation Technique". *Journal of Physical Oceanography, 31*, 2532-2536.

Thorne, P. W., J. R. Lanzante, T. C. Peterson, D. J. Seidel, and K. P. Shine, 2011: Tropospheric temperature trends: History of an ongoing controversy. *Wiley Interdisciplinary Reviews: Climate Change, 2*(1), 66-88.

Turk, F.J., R. Sikhakolli, P. Kirstetter, and S. L. Durden, 2015: Exploiting over-land OceanSat-2 scatterometer observations to capture short-period time-integrated precipitation. *Journal of Hydrometeorology*, *16*, 2519–2535.

Ueyama, R. and C. Deser, 2008: A Climatology of Diurnal and Semidiurnal Surface Wind Variations Over the Tropical Pacific Ocean Based on the Tropical Atmosphere Ocean Moored Buoy Array. *Journal of Climate, 21*, 593-607.

Verspeek, J., A. Stoffelen, M. Portabella, H. Bonekamp, C. Anderson, and J. F. Saldana, 2010: Validation and calibration of ASCAT using CMOD5.n, IEEE Trans. Geosci. Remote Sens., 48, 386–395.

Vogelzang, J., A. Stoffelen, A. Verhoef, and J. Figa-Saldaña, 2011: On the quality of high-resolution scatterometer winds. *Journal of Geophysical Research, 116* (C10), doi: 10.1029/2010JC006640.

Wentz, F.J., L. Ricciardulli, K.A. Hilburn and C.A. Mears, 2007: How Much More Rain Will Global Warming Bring? *Science*, *317*, 233-235.

Wentz, F.J. and Ricciardulli, L., 2011: Comment on "Global trends in wind speed and wave height". *Science*, *334*(6058), 905-905.

Wentz, F.J., 2013: SSM/I Version-7 Calibration Report. RSS Technical Report 011012, Remote Sensing Systems, Santa Rosa, CA, 46pp. Available online at http://www.remss.com/papers/tech_reports/2012_Wentz_011012_Version-7_SSMI_Calibration.pdf

Wentz, F.J. and L. Ricciardulli, 2013: Improvements to the Vector Wind Climate Record Using RapidScat as a Common Reference and Aquarius/SMAP for High Winds in Rain. RSS Technical Report 111313, Available online at

http://images.remss.com/papers/rsstech/2013_111313_Wentz_OVW_CDR.pdf

Wentz, F.J., 2015: A 17-year climate record of environmental parameters derived from the Tropical Rainfall Measuring Mission (TRMM) Microwave Imager. *Journal of Climate, 28*, 6882-6902.

Wentz, F.J. and D. Draper, 2016: On-orbit absolute calibration of the Global Precipitation Mission Microwave Imager. *Journal of Atmospheric and Oceanic Technology,* accepted pending revision.

WMO, 2011: Systematic Observation Requirements for Satellite-based Products for Climate Supplemental details to the satellite-based component of the Implementation Plan for the Global Observing System for Climate in Support of the UNFCCC (2010 Update), World Meteorological Organization, GCOS-154, 127pp.

Wood, R., M. Köhler, R. Bennartz and C. O'Dell, 2009: The diurnal cycle of surface divergence over the global oceans. *Quarterly Journal of the Royal Meteorological Society, 135*, 1484-1493.

Young, I.R., Zieger, S. and Babanin, A.V., 2011a: Global trends in wind speed and wave height. *Science*, *332*(6028), 451-455.

Young, I.R., A.V. Babanin, and S. Zieger, 2011b: Response to Comment on "Global trends in wind speed and wave height". *Science*, *334*(6058), 905-905.

Zeng, L., and R.A. Brown, 1998: Scatterometer observations at high wind speeds. *Journal of Applied Meteorology*, *37*, 1412-1420.

7. Appendix: QuikScat and RapidScat Evaluation

7.1 Introduction

This Appendix was prepared by the QuikScat/RapidScat Project at JPL. It first presents an evaluation of the non-spinning QuikScat data and then discusses the intercalibration of RapidScat using QuikScat. RapidScat experienced an anomaly on Aug 14, 2015 that drastically changed the calibration of the instrument. We present the calibration and stability of the instrument both before and after the anomaly. Finally, we discuss the usefulness of RapidScat as a climate data record.

7.2 Evaluation of QuikScat Stability: 2010 thru 2015

QuikScat stopped rotating in November 2009. Since this time, the instrument remains functional, but is pointed in a fixed direction. Without rotation, the measurement swath is only 25 km and the azimuthal diversity of the measurements was affected.

The Amazon rainforest provides a unique calibration target due to its relative stability in radar backscatter (Section 4.4). To assess the stability of QuikScat during the nominal operating phase (2000 – 2009) and during the non-spinning phase (> 2009) we use several regions of tropical rainforest located in South America and Africa. We also use stable ice covered regions of Antarctica. Table 7.1 shows the estimated drift rates for the radar backscatter over these three stable regions during the nominal phase. This table shows the remarkable stability of the instrument over nearly a decade. The small error bars in these estimates is possible due to the wide swath of QuikScat, which provided nearly daily samples, and due to the azimuthal variability, which was almost uniformly distributed during the nominal phase of operation.

Table 7.1 QuikScat Estimated Drift 2000 – 2009

	HH drift (dB/year)	HH drift error (dB/year)	VV drift (dB/year)	VV drift error (dB/year)
South America	-0.0061	+/- 0.0007 (1 σ_o)	-0.0056	+/- 0.0007 (1 σ_o)
Africa	-0.0042	+/- 0.0011 (1 σ_o)	-0.0025	+/- 0.0011 (1 σ_o)
Antarctica	-0.0003	+/- 0.0028 (1 σ_o)	-0.0002	+/- 0.0027 (1 σ_o)

After QuikScat stopped spinning, the precision of each backscatter measurement increased, since the number of radar independent samples per wind vector cell increased. The swath narrowed to 25 km, thereby reducing sampling, and the azimuth diversity decreased. It is important to assess the impact of the reduced sampling and azimuthal variability. To do so, we examined the γ_0, which is the σ_0 divided by the incidence angle, during the non-spinning phase. The γ_0 accounts for angular variations when volume scattering is present.

Figure 7.1 shows the γ_0 averaged over 3-day intervals since the start of 2010. Due to limitations of the non-spinning QuikScat, it is not possible to collect data simultaneously in both polarizations. The data were collected at incidence angles appropriate for OSCAT (before 2014) or RapidScat (after 2014), with a few QuikScat nominal incidence angle collections. This variation in incidence angles is accounted for, somewhat, by using γ_0 instead of σ_0. Nonetheless, it is likely that additional geophysical variability adds to the scatter or drifts estimated from these results.

Figure 7.1. γ_0 estimated over 3-day periods for HH (blue) and VV (green) polarizations. The lines are the drift estimates by fitting the entire time series (solid lines), or the time series stopping after 5 years of data collection (dashed lines), to study the sensitivity to fitting period.

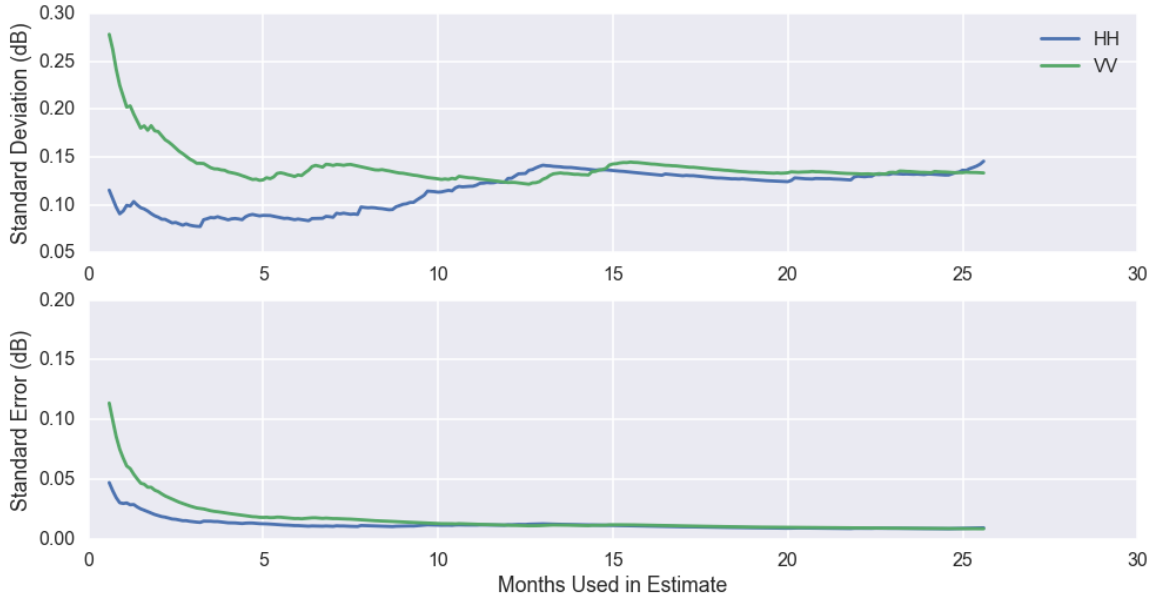

Figure 7.2. (Upper panel) Estimated standard deviation of backscatter cross-section for a period starting in 2010 and ending after a given number of months. (Lower panel) estimated standard error in the estimates (i.e., standard deviation divided by the square root of the number of samples used).

Figure 7.1 shows that both beams could be experiencing a small trend of about 0.02 dB/year variation in the mean cross section. However, these drifts could also be due to intrinsic variations in the Amazon, since the rainforest is known to be sensitive to the extreme El Niño conditions that started in 2015. To examine the impact of any geophysical variability, we fit the data through 2014, and observe a decrease in the drift rate in HH polarization, while VV remains essentially unaffected. Therefore, since QuikScat stopped spinning, one could say the absolute calibration of QuikScat has dropped by about 0.1dB. Some caution must be taken given in drawing this conclusion however given changes in the Amazon basin. Additional calibration techniques such as the histogram matching described below must be considered in parallel.

The upper panel in Figure 7.2 shows the standard deviation of the mean cross section derived as the averaging period increases. A stable estimate of the standard deviation is obtained after approximately 10 months of data, yielding similar standard deviation estimates for the 3-day averaged data of less than 0.14 dB. This quantity is greater than that observed during the nominal QuikScat mission, but still provides a good baseline for calibration.

What is the length of time over which data need to be collected before a stable estimate of the calibration can be obtained? To answer this question, we show the error estimate for the mean bias provided by the standard error in the lower panel of Figure 7.2. Achieving better than 0.05 dB bias estimates can be obtained using less than a month of continuous data collection (or two months of actual data collection, since each polarization must be collected separately). An estimate at the 0.01 dB level can be obtained after about 6 months of data collection. These estimates may be somewhat optimistic since, as shown in Figure 7.1, neighboring points may be correlated, likely due to seasonal variations in the cross section. As a rough guess, we estimate that one could achieve a better than 0.1 dB calibration after a month and reach better than 0.05 dB within 3-6 months using the rainforest as a calibration target.

7.3 Immediate Post-Launch Calibration of RapidScat using QuikScat

The initial calibration of RapidScat was completed using the ocean as a reference target using 2014 data. The over-ocean RapidScat σ_o measurements were adjusted to match QuikScat observations. The σ_o measurements for both sensors were collocated with ECWMF wind speed and directions between latitude 50^oS to 50^oN. The latitude restriction avoided ice contaminated regions. We also excluded RapidScat observations greater than $\pm1^o$ of the mean RapidScat incidence angles.

A histogram matching technique (Jaruwatanadilok et al, 2013) was used to find the σ_o differences between the two sets of measurements. This histogram matching technique is crucially important to obtain an accurate comparison between the two sensors. As shown in Jaruwatanadilok et al, when averaging normalized radar cross section (NRCS) values over the ocean from datasets that are not precisely collocated, the primary contribution to differences in the mean NRCS values is not the calibration differences but rather the differences in the wind speeds observed by the two sensors. Even if the measurements are precisely collocated (and thus the number of observations used is greatly reduced), differences in viewing geometry result in large apparent NRCS biases due to relative azimuth differences. The histogram matching technique detailed in Jaruwatanadilok, et al eliminates biases due to different wind speed and relative azimuth distributions by using weighted averaging that normalizes the contribution of measurements from different wind speed and relative azimuth regimes. The results of this procedure are average σ_o values of both QuikScat and RapidScat that have been adjusted to correct for sensor-dependent and temporal variation in wind speed and wind-relative azimuth angle. This histogram matching method is done on monthly or biweekly data, and thus it can be used to both calibrate σ_o and track the drift of the σ_o over time. Variation in NRCS bias due to rain is not corrected by

the histogram matching technique. However, the impact of rain is limited by its infrequency in the data and the fact that only differences in rain amounts will affect the analysis. So long as both sensors observe a similar amount of rain-contaminated data there is no issue. Table 7.2 gives the average σ_o values for QuikScat and RapidScat along with the incidence angles and time periods used. There are five separate months of QuikScat V-pol data and the standard deviations for these 5 months is given in Table 7.2. Figure 7.3 compares the QuikScat and the uncalibrated RapidScat σ_o measurements as a function of wind speed.

Table 7.2: 2014 QuikScat and RapidScat data used in calibration and their incidence angle behaviors

	Period	Incidence angle		σ_o (dB)	
		average	STD	average	STD
H-pol					
QuikScat	2014/09/12 – 2014/10/24	47.80	0.07	-22.75	
RapidScat	2014/10/03 – 2014/10/13	48.79	1.05	-22.04	
QuikScat - RapidScat (i.e., correction added to RapidScat)		-0.99		-0.70	
V-Pol					
QuikScat	2014/04/08 – 2014/09/12	56.67	0.09	-20.78	0.02[note1]
RapidScat	2014/10/03 – 2014/10/13	55.20	1.09	-19.26	
QuikScat - RapidScat (i.e., correction added to RapidScat)		1.47		-1.52	
Note1: This is the standard deviation of 5 separate months of QuikScat V-pol data					

Despite the difference of 1-1.5 degrees between the mean QuikScat and RapidScat incidence angles, no attempt was made initially to account for incidence angle dependence in the correction. The mean difference in incidence angle between the two sensors was similar to the standard deviation of incidence angle for RapidScat and the time period for the comparison was short, so further calibration refinement was left until such time as sufficient data at similar incidence angles was available from both sensors. As we shall see in the next section, the initial calibration turned out to be an accurate calibration constant for the RapidScat mission prior to the August 14, 2015 anomaly.

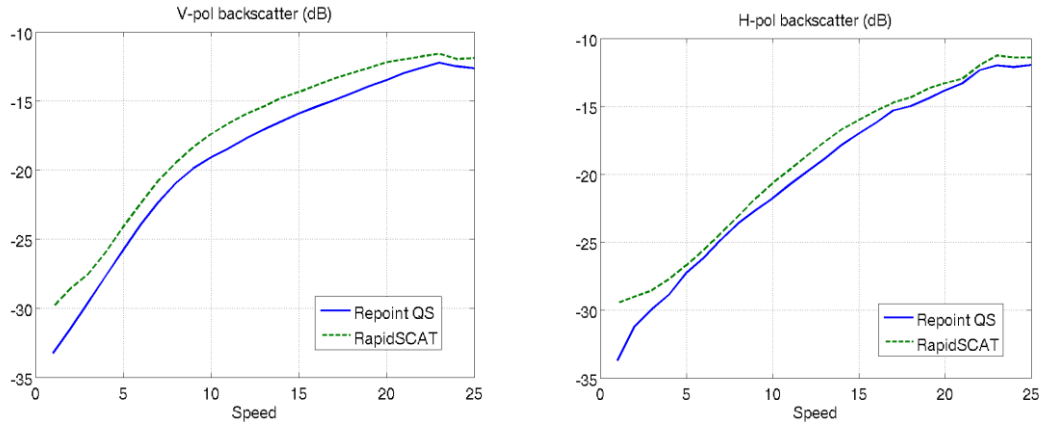

Figure. 7.3. The QuikScat and RapidScat σ_o measurements plotted as a function of ECMWF wind speed.

7.4 Comparison of RapidScat and QuikScat Data

The σ_o offsets listed in Table 7.2 were applied to the RapidScat data, and then the performance of these offsets, which were derived just using 2014 observations, were validated using 2015 data. The same histogram matching technique used for the initial calibration was also used to analyze the 2015 data. Also in 2015, QuikScat was commanded to better match the RapidScat incidence angles and H-pol and V-pol QuikScat data was acquired alternately every 2 weeks. Table 7.3 shows the bias computed for each two-week period during 2015. The average incidence angle of the QuikScat and RapidScat data differed by less than 0.2 degrees throughout 2015 with the exception of the time period from 8/28/2015 to 9/11/2015 when they differed by 0.33 degrees. Table 7.4 documents the incidence angles.

Table 7.3. RapidScat Versus QuikScat Bias During 2015

Period	Pol	QuikScat	RapidScat		
		Average	State	Average	Bias
04/10 – 04/28	H	-23.1422	HighSNR-LowPitch	-23.2535	-0.1113
04/28 – 05/08	V	-20.5999	HighSNR-HighPitch	-20.8834	-0.2835
05/08 – 05/22	H	-23.2955	HighSNR-HighPitch	-23.3603	-0.0648
05/22 – 06/05	V	-20.8294	HighSNR-HighPitch	-21.0014	-0.172
06/06 – 06/19	H	-23.3657	HighSNR-HighPitch	-23.2690	+0.0967
06/16 – 07/03	V	-20.9041	HighSNR-HighPitch	-20.8687	+0.0354
07/03 – 07/17	H	-23.3441	HighSNR-LowPitch	-23.3093	+0.0348
07/17 – 07/31	V	-20.8077	HighSNR-LowPitch	-20.9554	-0.1477
07/31 – 08/14	H	-23.2604	HighSNR-LowPitch	-23.2723	-0.0119
08/14 – 08/28	V	-20.7609	LowSNR-LowPitch	-20.9547	-0.1938
08/28 – 09/11	H	-23.2872	LowSNR-LowPitch	-22.9836	+0.2399
09/11 – 09/25	V	-20.8378	HighSNR-HighPitch	-20.8838	-0.0460
09/25 – 10/09	H	-23.2733	HighSNR-LowPitch	-23.2341	+0.0392
10/09 – 10/23	V	-20.9273	LowSNR-LowPitch	-20.7651	+0.1622
10/23 – 11/11	H	-23.3541	LowSNR-LowPitch	-22.9231	+0.4310

Table 7.3 shows the RapidScat minus QuikScat NRCS bias during 2015. The table contains shaded lines to identify anomalous time periods due to 1) spacecraft pitch > 1.5 degrees (blue) or 2) instrument gain anomaly with SNR reduced by 10 dB (green). The RapidScat low SNR data used for the comparison was first recalibrated by adding 14.45 dB to make it consistent with high SNR mode data as discussed in section 7.4.3 below. For nominal (HighSNR) RapidScat data with spacecraft pitch less than 1.5 degrees, the mean bias was -0.0608 dB. For pitch>1.5 degrees, the mean bias was -0.0724 dB. For the low SNR mode data, the mean bias is 0.1598 dB.

From this analysis, we conclude that the high SNR (nominal) mode RapidScat data is closely calibrated to QuikScat within 0.1 dB. The low SNR mode (anomalous) data appears to be biased high with respect to QuikScat by 0.15 dB on average with a possible trend. The next section provides further analyses of the stability of RapidScat data.

Table 7.4: Incidence angles in degrees for 2015 QuikScat and RapidScat data

period	pol	QuikScat		RapidScat	
		average	STD	average	STD
04/10 – 04/28	H	48.7304	0.0506	48.7516	1.8449
04/28 – 05/08	V	54.9787	0.0664	55.1347	1.7623
05/08 – 05/22	H	48.7309	0.0529	48.7409	1.7694
05/22 – 06/05	V	54.9793	0.0677	54.9133	2.4389
06/06 – 06/19	H	48.7302	0.0526	48.7781	2.1041
06/16 – 07/03	V	54.9777	0.0649	55.1478	1.3748
07/03 – 07/17	H	48.7297	0.0495	48.6994	0.9853
07/17 – 07/31	V	54.9770	0.0624	55.0451	1.4443
07/31 – 08/14	H	48.7292	0.0496	48.7945	2.1178
08/14 – 08/28	V	54.9782	0.0648	54.9126	2.2822
08/28 – 09/11	H	48.7303	0.0524	48.4048	3.9769
09/11 – 09/25	V	54.9783	0.0677	55.1127	0.9148
09/25 – 10/09	H	48.7300	0.0530	48.7360	0.9229
10/09 – 10/23	V	54.9778	0.0662	55.1216	0.9246
10/23 – 11/11	H	48.7293	0.0499	48.7126	0.8596

7.4.1 RapidScat Stability Validation over Ocean and Land

Average daily sigma-0 anomalies over land from 25 degrees S latitude to 25 degrees N latitude were computed using the expected NRCS and variance on NRCS. The anomaly is an average of the daily difference from the expected NRCS value weighted by the inverse of the standard deviation of NRCS, so that regions with little change in NRCS are preferred. The anomaly so computed is the most likely offset in dB given mutually independent Gaussian distributions in NRCS for each point on the ground. Similar anomalies were also computed for QuikScat for year 2007 and 2008 when it was operating nominally. Figure 7.4 shows the expected NRCS value in dB and the standard deviation as a percentage computed over the portion of the RapidScat mission prior to the August 14, 2015 gain anomaly.

$$A(t_1, t_n) = 10\ \log_{10}\left(\frac{\sum_{i=1}^{n}\frac{\sigma_0(t_i)}{\sqrt{Var(\sigma_0|x(t_i))}}}{\sum_{i=1}^{n}\frac{E(\sigma_0|x(t_i))}{\sqrt{Var(\sigma_0|x(t_i))}}}\right) \quad (7.1)$$

Equation 7.1 shows the calculation performed to determine the NRCS anomaly, A(t0,t1) in dB given the individual linear scale (not in dB) NRCS values $\{\sigma_0(t_i)\}$ obtained during the time interval $[t_1,t_n]$, and the expected value (mean) and variance conditional on the location of each measurement on the ground $x(t_i)$. Mean and variance were also computed from linear scale NRCS values. For RapidScat the expected values were computed using all data from Oct 3, 2014 to August 14, 2015. For QuikScat expected values were computed using all data from calendar year 2008. Figure 7.5 shows the daily anomaly for the HH co-pol NRCS measurements from RapidScat as compared to the same measurements for QuikScat in years 2007 and 2008.

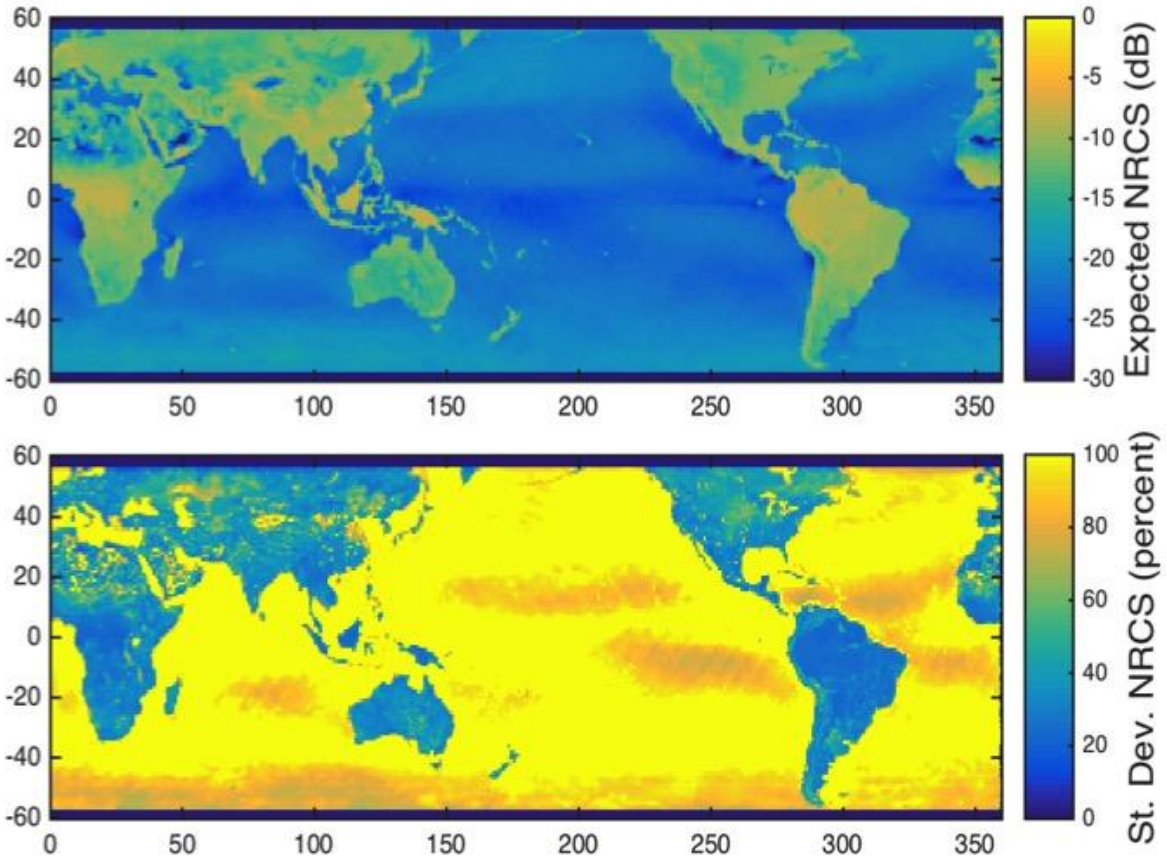

Figure 7.4. RapidScat Expected VV NRCS in dB and normalized standard deviation as a percentage from October 3, 2014 through August 14, 2015.

From Figures 7.5 and 7.6 we can draw several conclusions about the relative accuracy of QuikScat and RapidScat for land-based cross-calibration of NRCS values with other scatterometers. First, RapidScat is substantially more variable than QuikScat during its nominal (antenna spinning) mission. For VV polarization, standard deviation of RapidScat daily anomalies is 0.16 dB as compared to 0.04 dB for QuikScat. For HH polarization, the standard deviation of RapidScat daily anomalies is 0.17 dB as compared to 0.06 dB for QuikScat. Second, the period when the pitch of the International Space Station is more than 1.5 degrees from nadir pointing have larger anomalies. Such data needs further refinement in calibration or should be excluded from cross-calibration analyses. Finally there may be an increasing trend in the low SNR mode RapidScat bias. Further study is needed to see if this trend is erroneous or due to the variation in local time of day and seasonal variation.

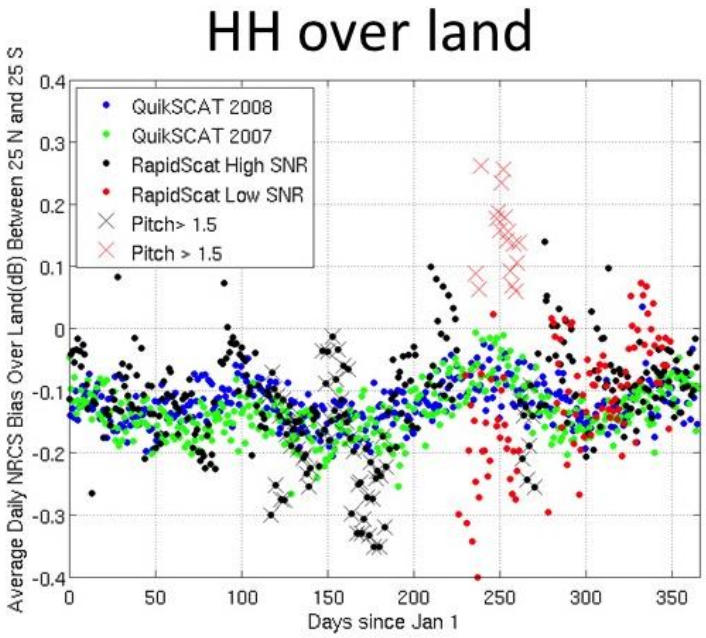

Figure 7.5. Daily land-based HH co-polarized RapidScat NRCS anomaly versus day of year as compared with QuikScat. A -0.3 dB correction has been applied to RapidScat data in low SNR mode in addition to the +14.45 dB initial low SNR offset for a total of +14.15 dB. The monthly periodic variation in the RapidScat data is due to the variation in local time-of-day. Only measurements between 25°N and 25°S latitude over land were used in the calculation. Locations with expected NRCS less than -15 dB were excluded from the calculation to minimize the effect of random measurement noise. The boundary effects resulting from the omission of this data is the cause of the -0.1 dB constant offset in the anomaly values.

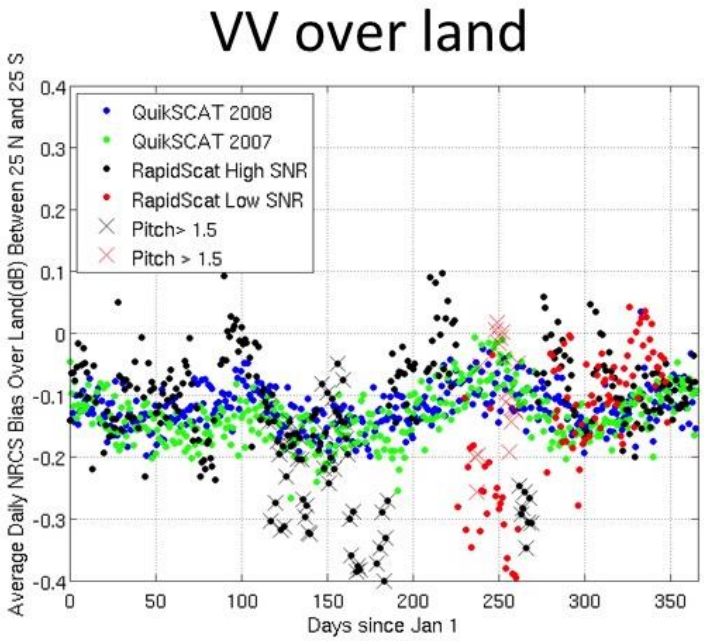

Figure 7.6. Daily Land-based VV co-polarized RapidScat NRCS Anomaly versus day of year as compared with QuikScat. A -0.3 dB correction has been applied to RapidScat data in low SNR mode in addition to the +14.45 dB initial low SNR offset for a total of +14.15 dB.

In addition to land-based studies, RapidScat NRCS values can also be compared over ocean by utilizing the geophysical model function (NSCAT2014) developed by Ricciardulli and Wentz (2014). The geophysical model function returns a NRCS value as a function of polarization, incidence angle, angle between instrument look vector and wind direction, and wind speed. For each RapidScat measurement collocated with the WindSat radiometer, a "model" NRCS value can be computed by applying the GMF to the WindSat wind speed and the ECMWF wind direction. For each day, an average difference between the model and measured NRCS values are computed as shown in Figures 7.7 and 7.8 for VV and HH respectively. These comparisons show a large monthly periodic variation due to the variation of local-time-of-day for RapidScat and thus variation in the geographical locations and wind speed regimes where WindSat and RapidScat overlap. Unlike in Figures 7.5 and 7.6, the additional -0.3 dB low SNR mode calibration correction was not applied. Therefore, there is a 0.3 dB bias between the black points from October-December 2014 (after day 270) and the red points from October to December 2015. These plots illustrate the challenge in using radiometer wind speeds and NWP directions to calibrate a Ku-band scatterometer. While this problem is obvious for RapidScat, which has variable local-time-of day observations, the same effect will impart an overall (unknown) bias when using a radiometer to cross-calibrate a sun-synchronous scatterometer.

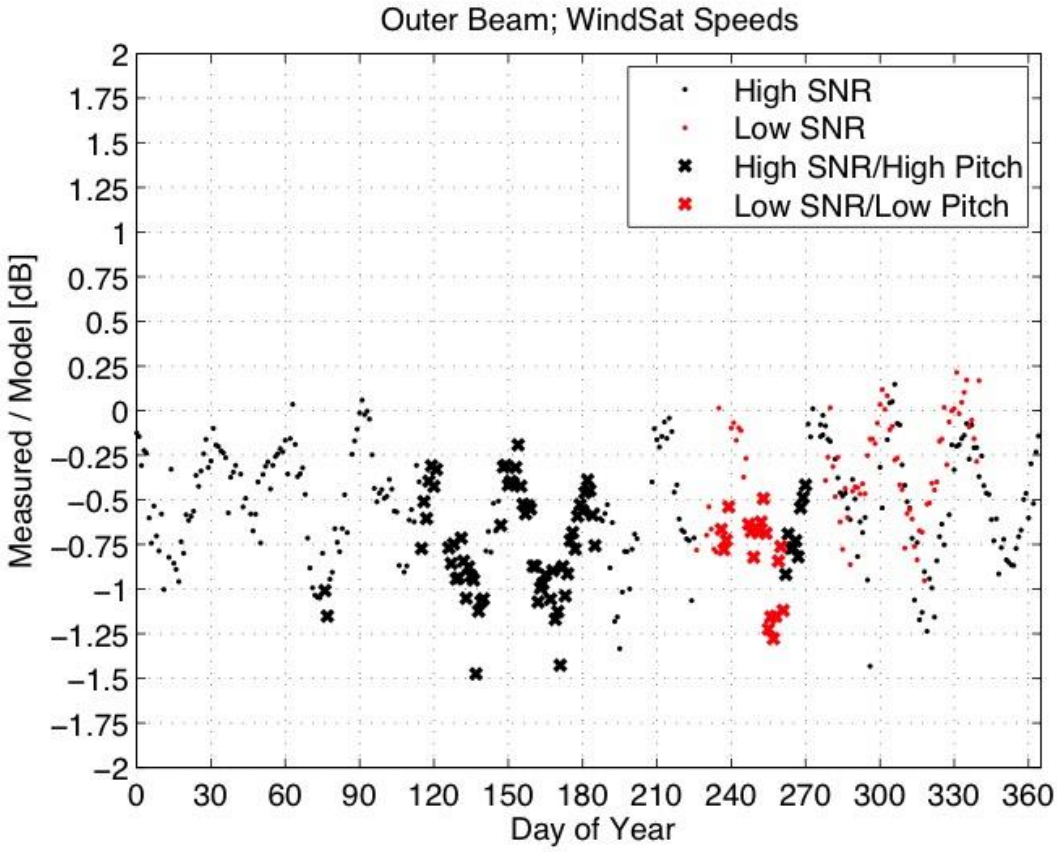

Figure 7.7. Estimated VV RapidScat NRCS bias in dB by comparison with WindSat speeds and ECMWF direction using the NSCAT-2014 GMF.

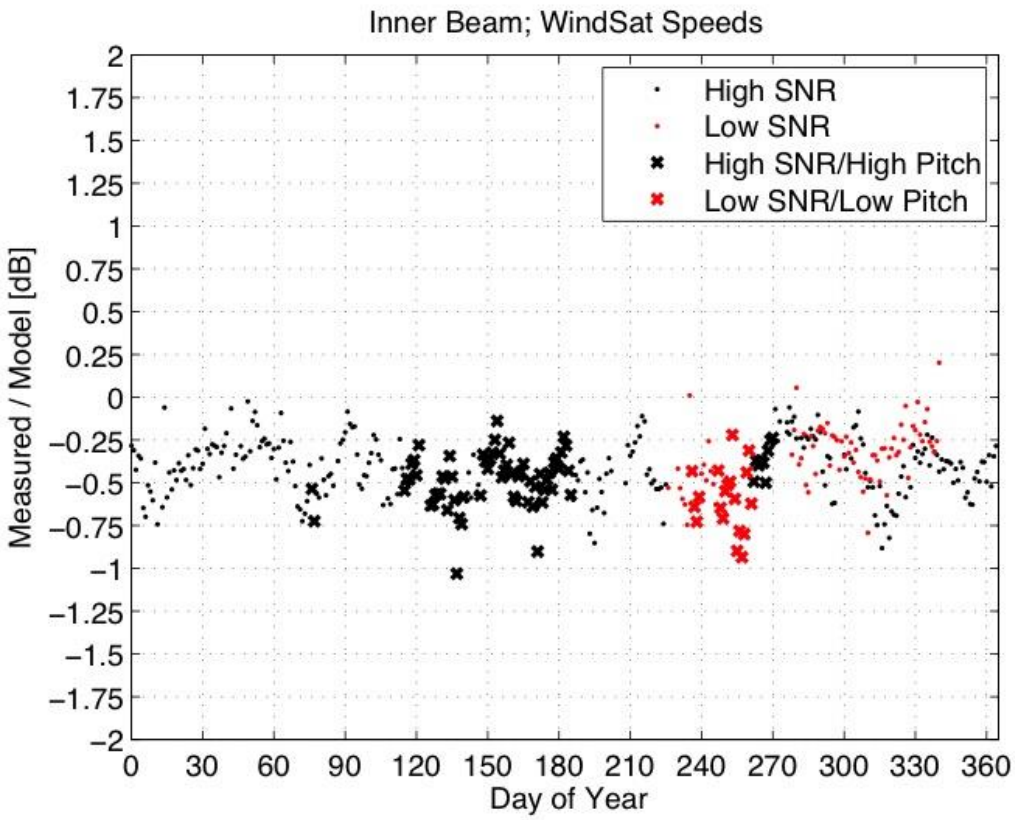

Figure 7.8. Estimated HH RapidScat NRCS bias in dB by comparison with WindSat speeds and ECMWF direction using the NSCAT-2014 GMF.

Figure 7.9 depicts fits of the RapidScat trend in NRCS over the Amazon. Figure 7.9 was produced using the same technique used to estimate trends from QuikScat non-spinning data in section 7.2. See figure 7.1 for comparison. Systematic errors due to spacecraft pitch, short time baseline, and local-time-of-day variation make estimating the RapidScat trend difficult. Even without considering systematic error, the formal error bars are 5 to 10 times larger than those for QuikScat. The -0.3 dB correction to the low SNR mode data was not included here. Without that correction, including the low SNR mode data increases, the estimated trends by 0.1-0.2 dB per year.

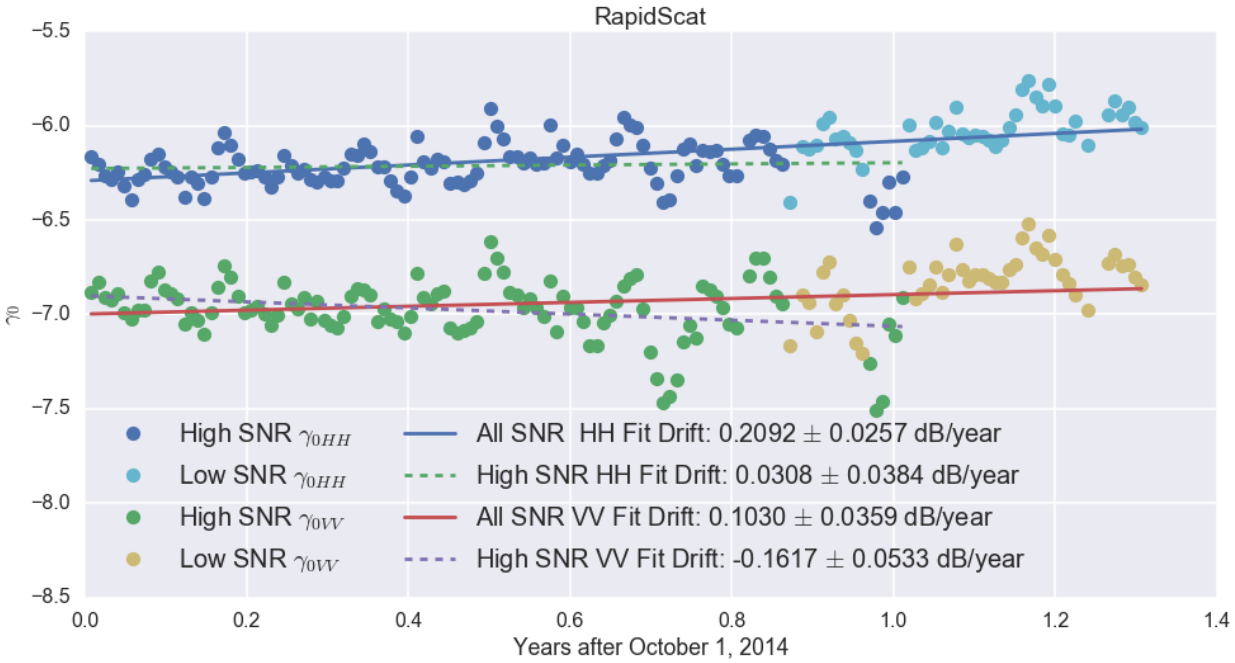

Figure 7.9. Estimate of RapidScat γ_0 trends computed from Amazon data. Dotted line trends omit low SNR data which are biased 0.3 dB high (computed using the original 14.45 dB recalibration value rather than the improved version, 14.15 dB). Solid line trends include the entire RapidScat dataset and thus show an erroneously increasing trend. Notice that the local-time-of-day variation in RapidScat contributes a large periodic signature not seen in the QuikScat data record (Figure 7.1). If two scatterometers with different local-times-of-day are intercalibrated over the Amazon, biases can result. The variable local-time-of-day of RapidScat observations enables the removal of such calibration biases.

7.4.2 RapidScat Wind Validation

In this section, we present the RapidScat wind speed and direction error statistics with respect to ECMWF, buoys and radiometers (speed only). Figure 7.10 depicts the speed bias, RMS speed difference, and RMS direction difference between the RapidScat High SNR mode winds and the ECMWF winds. The percentages of the RapidScat wind vectors within 45 degrees of the ECMWF direction are also plotted. Two different versions of the RapidScat wind retrievals are shown: 1) footprint and 2) slice wind retrievals. The footprint retrievals are produced from 25-km resolution full antenna footprint data. These retrievals are robust to errors in the knowledge of the spacecraft attitude or antenna gain patterns. The slice retrievals are performed using higher-resolution "slice" measurements in which radar power is broken up into range-to-target bins to improve resolution. These measurements and the retrievals produced from them are more prone to systematic error. For this reason footprint retrievals are preferred for long term trend estimation, cross calibration, and other applications where tenths of a dB or tenths of a m/s matter. RapidScat high SNR mode performance with respect to ECMWF is similar to the performance of QuikScat (Fore et al, 2014). Figure 7.11 reports the same error statistics shown in Figure 7.10 but for the low SNR mode RapidScat data. The slight differences in performance as compared to High SNR mode data is due primarily to winds between 3 and 5 m/s. Figure 7.12 shows the bias of the RapidScat retrieved directions with respect to ECMWF. This metric was typically not reported for QuikScat as it was negligible. It is a small error for RapidScat as well (< 2 degrees for footprints, < 4 degrees for slices), but because it has a discontinuity in the middle of the RapidScat

swath, it is problematic for derivative wind fields. The likely cause of this problem is errors in the knowledge of the RapidScat antenna gain patterns. Further study is needed to correct this problem. Figure 7.13 compares speed and direction errors for both modes with respect to ECMWF as a function of wind speed to illustrate that the difference in performance is indeed at low winds. Figures 7.14 (footprints) and 7.15 (slices) show RapidScat High SNR mode wind speed and direction errors with respect to buoys. Similar QuikScat metrics from October 2008-April 2009 (when it was spinning) are shown for comparison. There is little difference between the buoy comparisons for QuikScat and RapidScat high SNR mode data. Buoy metrics for Low SNR mode data were not computed because insufficiently many buoy colocations were available.

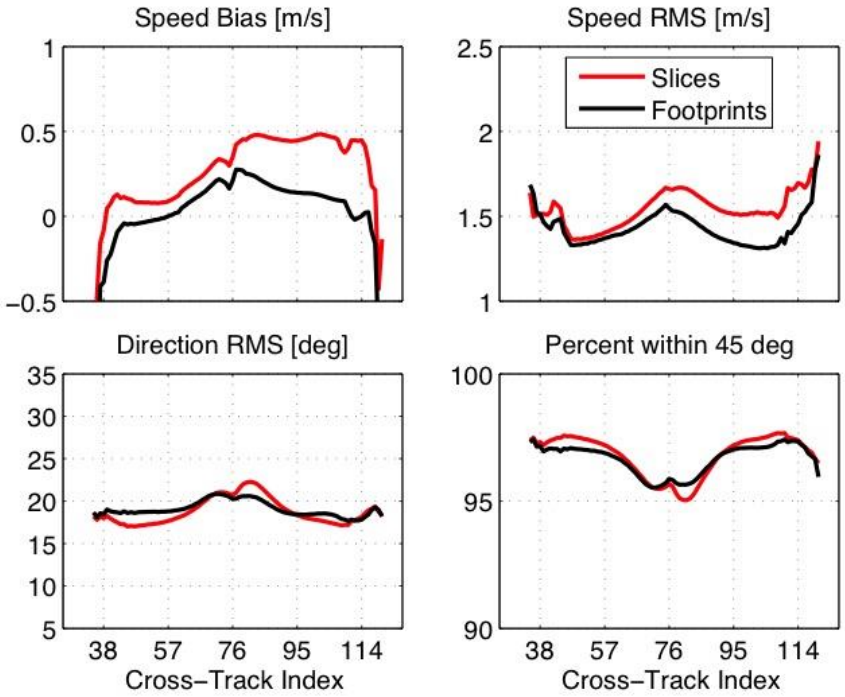

Figure 7.10. RapidScat Wind performance statistics vs. ECMWF for 12.5-km gridded winds using whole footprints (black) or range-compressed slices (red). The x-axis for each plot is in the cross-track position in the swath in 12.5-km units. Slice NRCS measurements have systematic calibration errors due to errors in the knowledge of the antenna pattern and the spacecraft attitude. Full footprint NRCS measurements are much less sensitive to these errors. For this reason footprint NRCS are preferable for cross-calibration. The performance shown is for High SNR mode data.

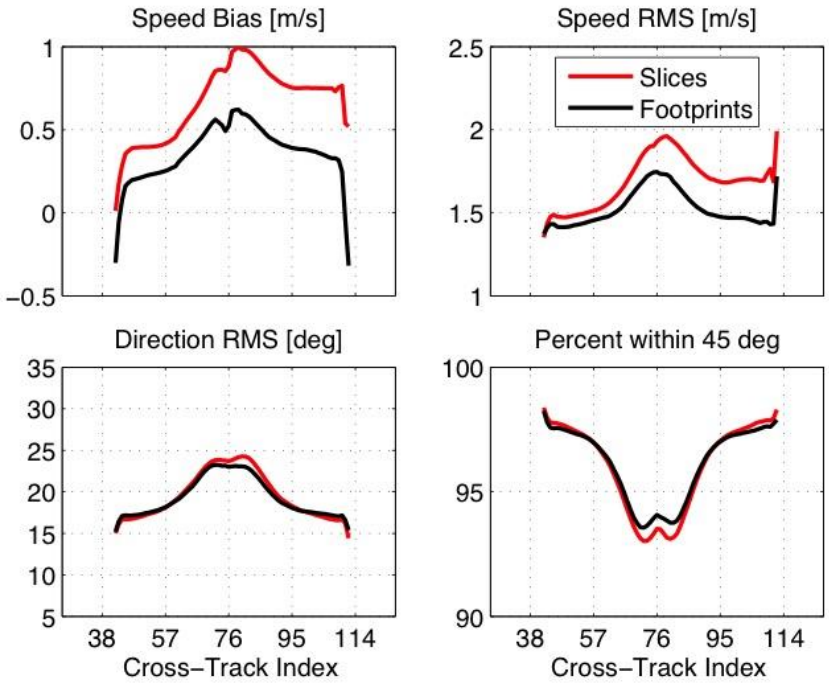

Figure 7.11. RapidScat Wind Performance Statistics vs. ECMWF for 12.5-km gridded winds using whole footprints (black) or range-compressed slices (red). The performance shown is for Low SNR mode data.

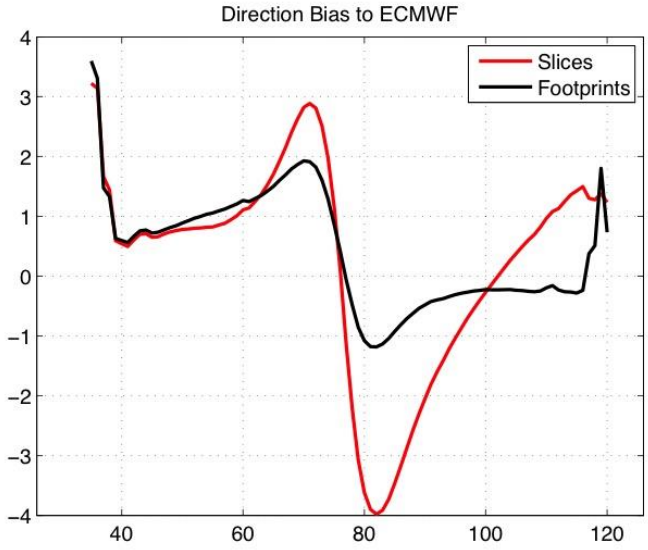

Figure 7.12. RapidScat direction bias with respect to ECMWF. Y-axis is in degrees. X-axis is cross track distance in units of 12.5-km. Although the bias is small, the discontinuity in the middle of the swath affects the accuracy of derivative wind fields especially for slice processing. The performance shown is for High SNR mode data.

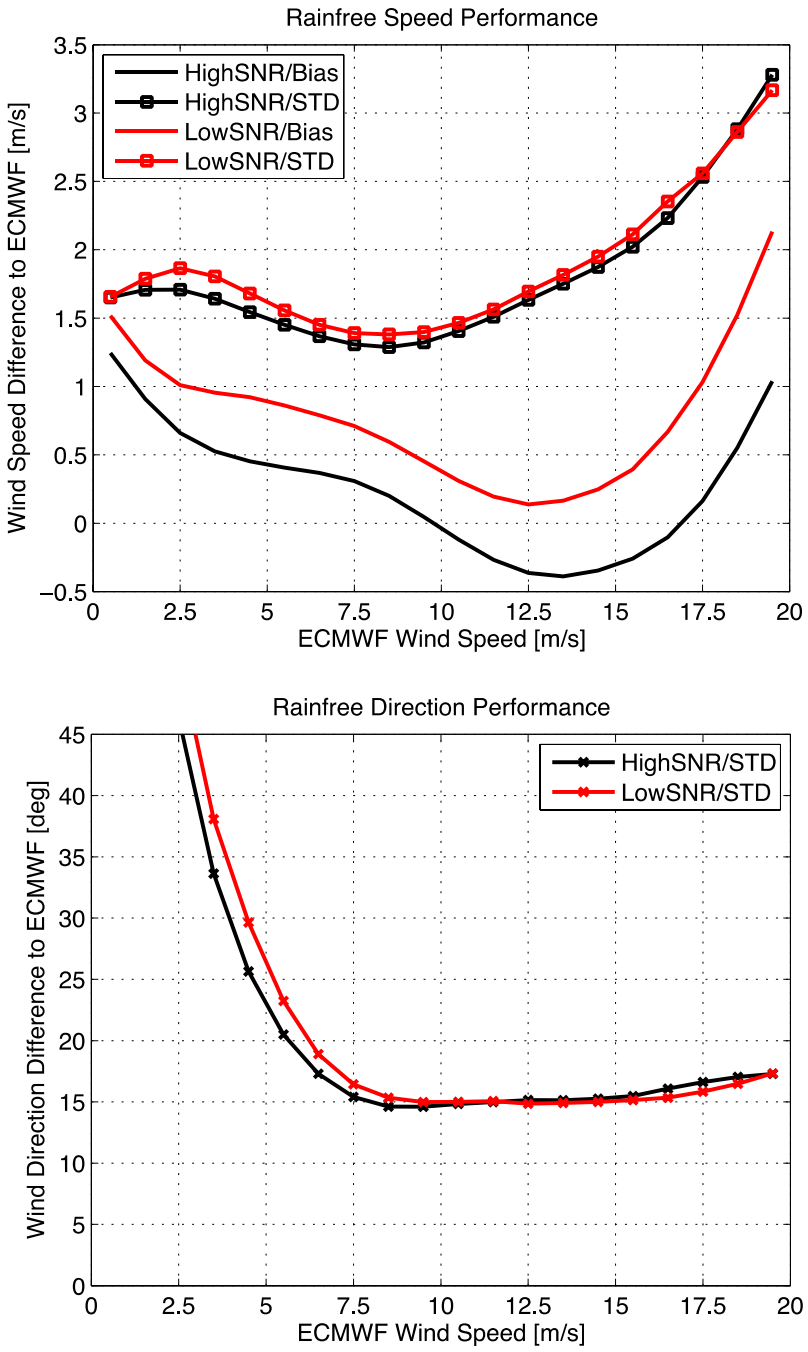

Figure 7.13. Speed and Direction Performance Comparison of the two RapidScat modes. Wind speed (top panel) and wind direction (bottom panel) difference statistics with respect to ECMWF are shown for ECMWF wind speeds below 20 m/s. For low ECMWF wind speeds, all sources of wind directions are inaccurate including those from ECMWF.

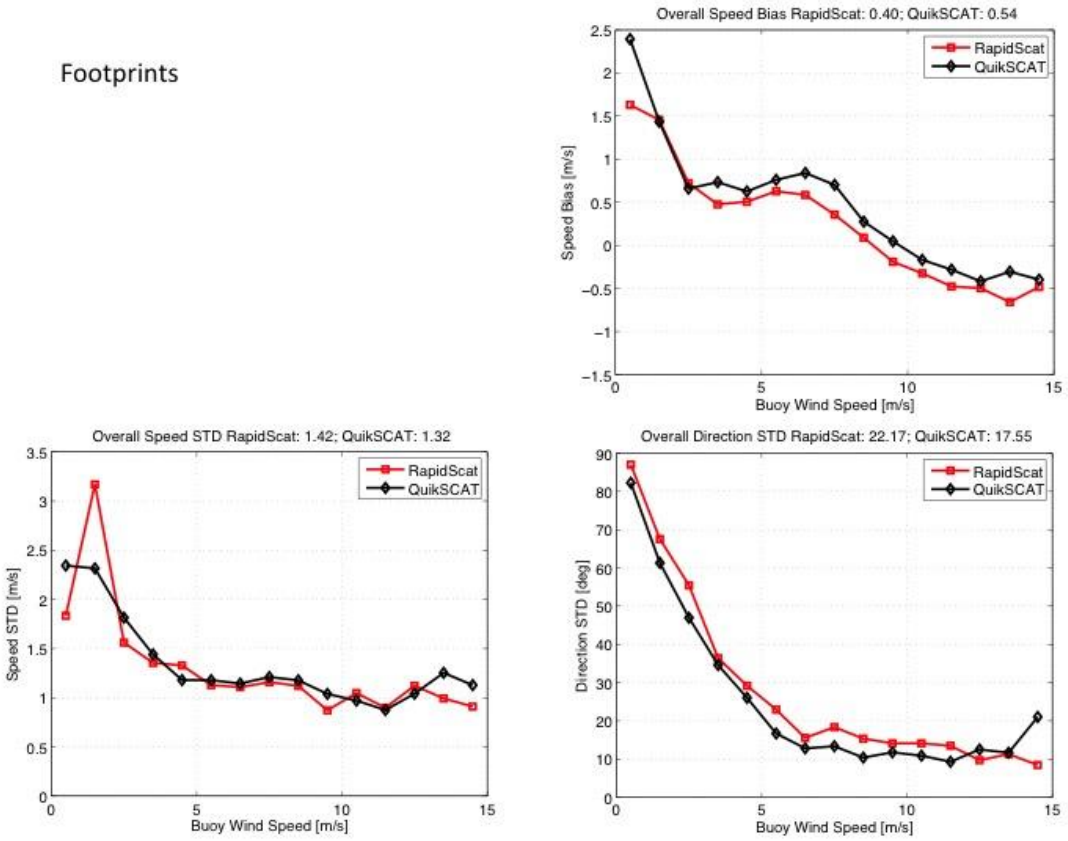

Figure 7.14. RapidScat wind difference metrics vs. buoys (footprint winds). The performance shown is for High SNR mode data.

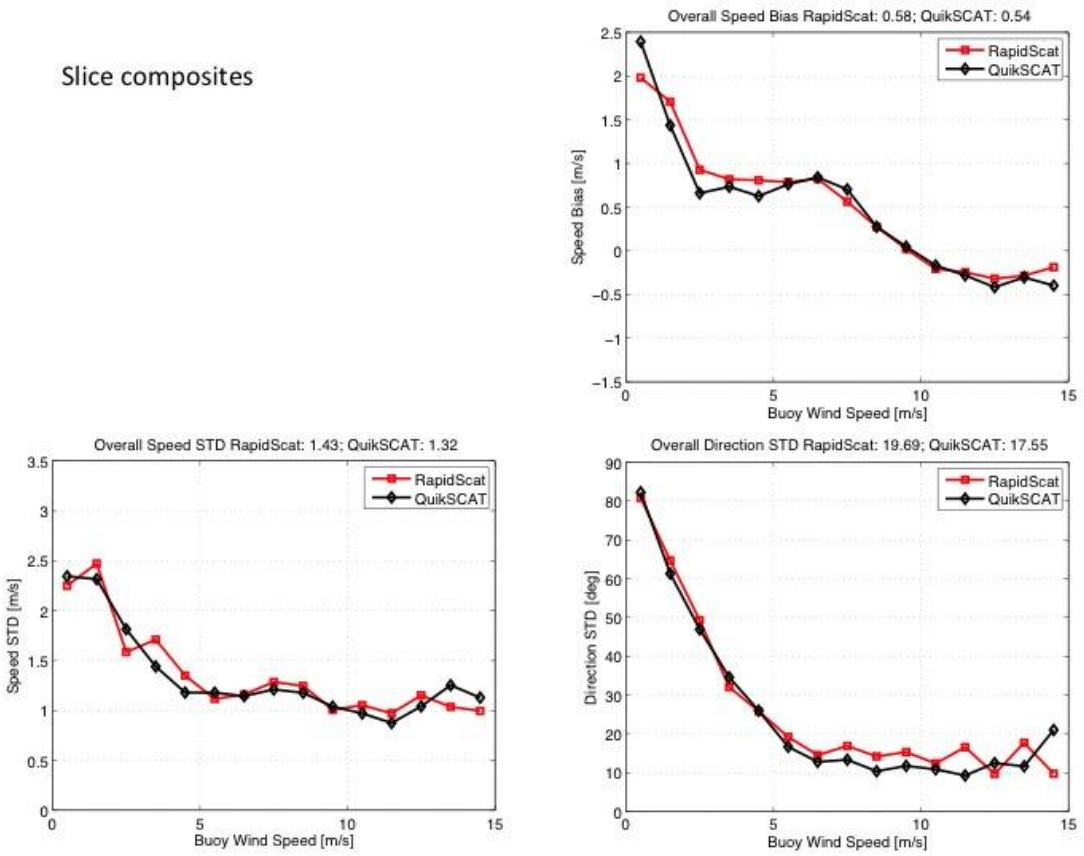

Figure 7.15. RapidScat wind difference metrics vs. buoys (slice winds). The performance shown is for High SNR mode data.

In addition to comparisons with ECMWF and buoys, we also compare RapidScat footprint wind speeds with collocated radiometer data. Figures 7.16, 7.17, and 7.18 show two dimensional histograms of RapidScat wind speed (y-axis) with three radiometer wind speeds (x-axis). WindSat, GMI, and AMSR2 radiometer wind speeds are shown in Figures 7.16, 7.17, and 7.18 respectively. Four plots are depicted in each figure, one plot for each of four time periods: 1) the original High SNR mode period from October 3 2014-August 14, 2015, 2) the first low SNR mode anomaly period August 14- September 18 2015, 3) the second High SNR mode time period September 18 – October 6, 2015, and 4) the second anomalous Low SNR mode time period October 6 2015 to Nov 15, 2015. Additional rain-flagging is performed using 90-minutes colocated radiometer rain observations. Biases and standard deviations are shown for each plot. The standard deviations are in the range 0.86-1.07 m/s for all but one case (Low SNR mode 1, GMI comparison). The biases are consistently -0.2 to -0.3 m/s for High SNR mode data (RapidScat wind speeds less than the radiometer speeds.) This bias is explained by a 0.25 dB sigma-0 offset used in the generation of the GMF by RSS that was not utilized in the JPL wind retrievals. No such bias was found for the slice wind retrievals from High SNR mode data probably due to an offsetting error in the NRCS slice calibration. Low SNR mode footprint wind speeds are generally unbiased compared to the radiometers varying from -0.08 m/s to + 0.06 m/s for all cases but one (again, the low SNR time period 1 GMI comparison.) The difference in bias between the two SNR modes is explained by the fact that -0.3 dB correction has not yet been applied to the low SNR mode data used in the retrievals.

All the figures in this section make use of RapidScat data that has been marked as rain-free by the rain flagging algorithm. The rain flagging algorithm is somewhat degraded for low SNR data as compared to high SNR data because the RapidScat brightness temperature values are not usable in the low SNR mode. To compensate for this problem the rain flagging method used in low SNR mode flags a larger percentage of the data (3% instead of 2%) as rain contaminated and thus has a higher false alarm rate. Additionally, the extreme edges of the swath (75-km on each side) cannot be flagged for rain without brightness temperatures, so for low SNR mode the edges of the swath need external information (e.g. co-located radiometer data) to determine whether or not the wind vectors are contaminated by rain.

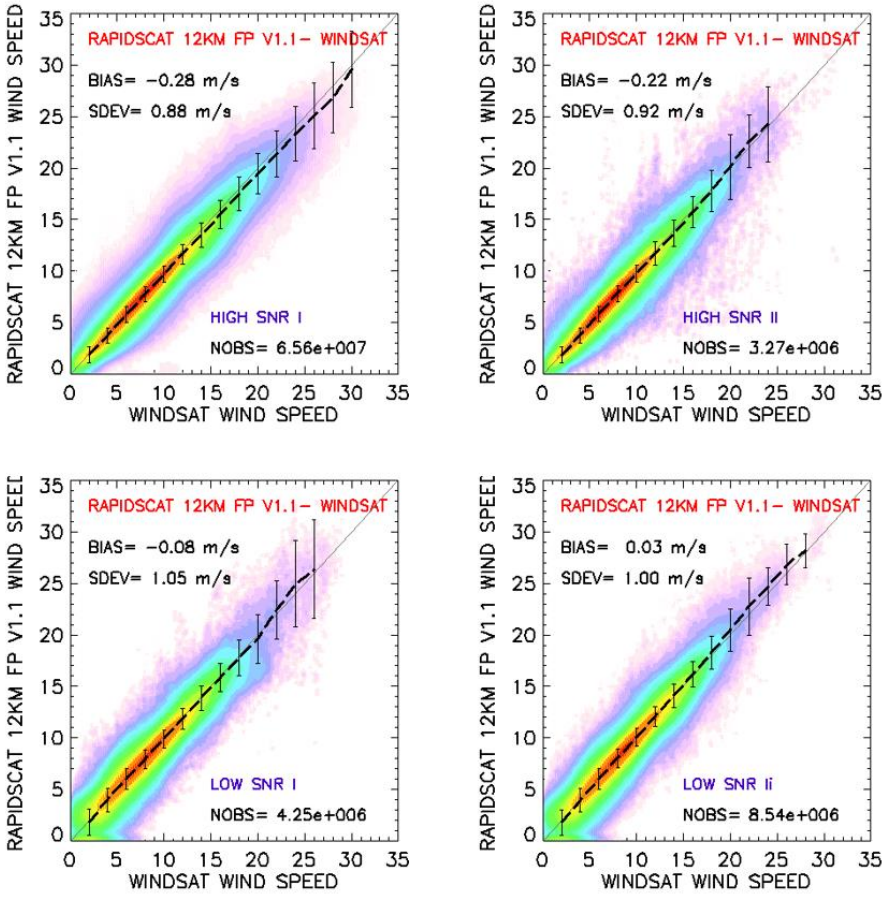

Figure 7.16. RapidScat/WindSat rain-free wind speed joint probability distribution functions (PDFs). The four panels refer to the four distinct periods in the RapidScat state. Top panels: (left) High SNR mode I, Oct 3 2014-Aug 14 2015 and (right) High SNR mode II, Sept 18 2015-Oct 6 2015. Bottom panels: (left) Low SNR mode I, Aug 14–Sept 18 2015 and (right) Low SNR mode II, Oct 6 2015-current. For this analysis of the RapidScat footprint winds, only data from Oct 6 to Nov 15 2015 where used.

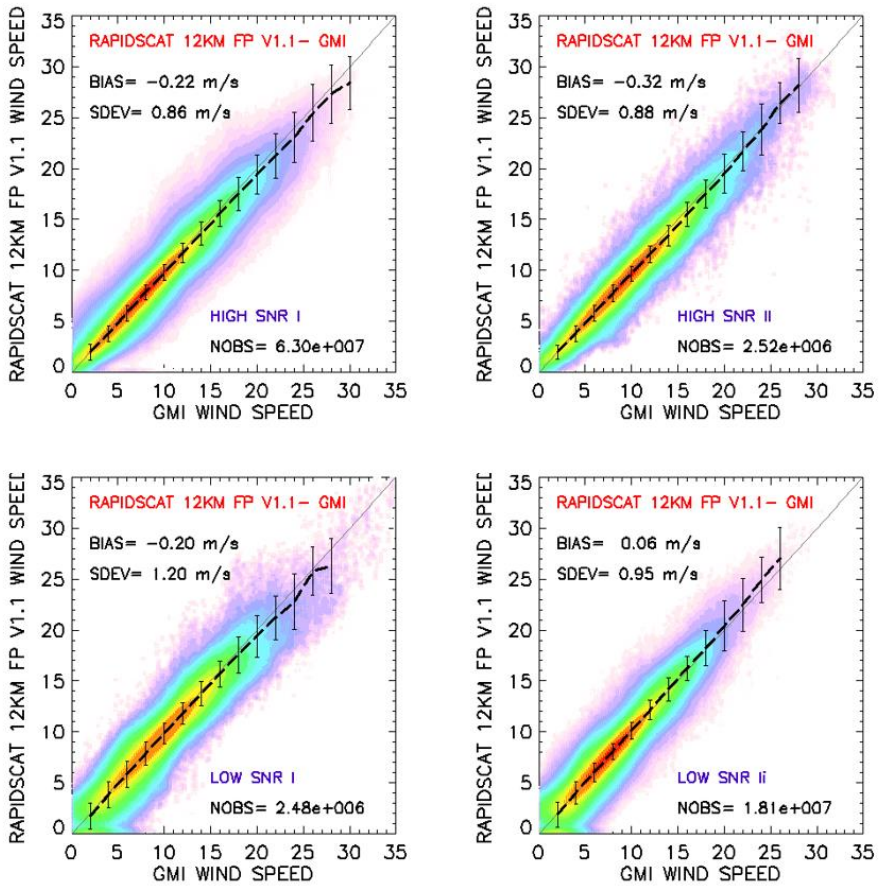

Figure 7.17. Same as Fig. 7.16, but for RapidScat/GMI rain-free wind speed two-dimensional histograms.

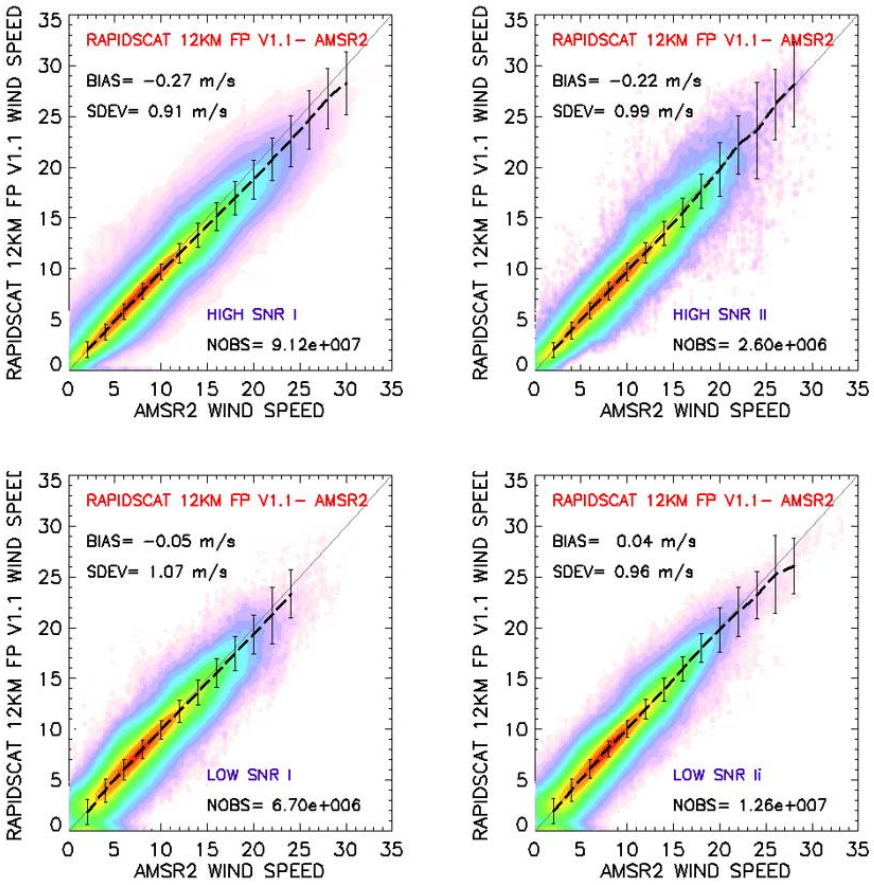

Figure 7.18. Same as for Fig. 7.16, but for RapidScat/AMSR2 rain-free wind speed two-dimensional histograms.

7.4.3 Recalibration of RapidScat due to Anomaly

On August 14, 2015, the observed echo power of RapidScat dropped by a factor of 100. Fortunately, much of this drop was an absolute change in gain that affects both signal and noise, so the actual loss in dynamic range was "only" a factor of 10. Because of the large variation in NRCS with wind speed a loss in signal to noise-ratio (SNR) of 10 dB is only noticeable for winds with speeds below 6 m/s. Figure 7.19 illustrates the August 14, 2015 anomaly and its reversal on September 18, 2015. The gain anomaly reasserted itself on October 6, 2015 and has remained until now.

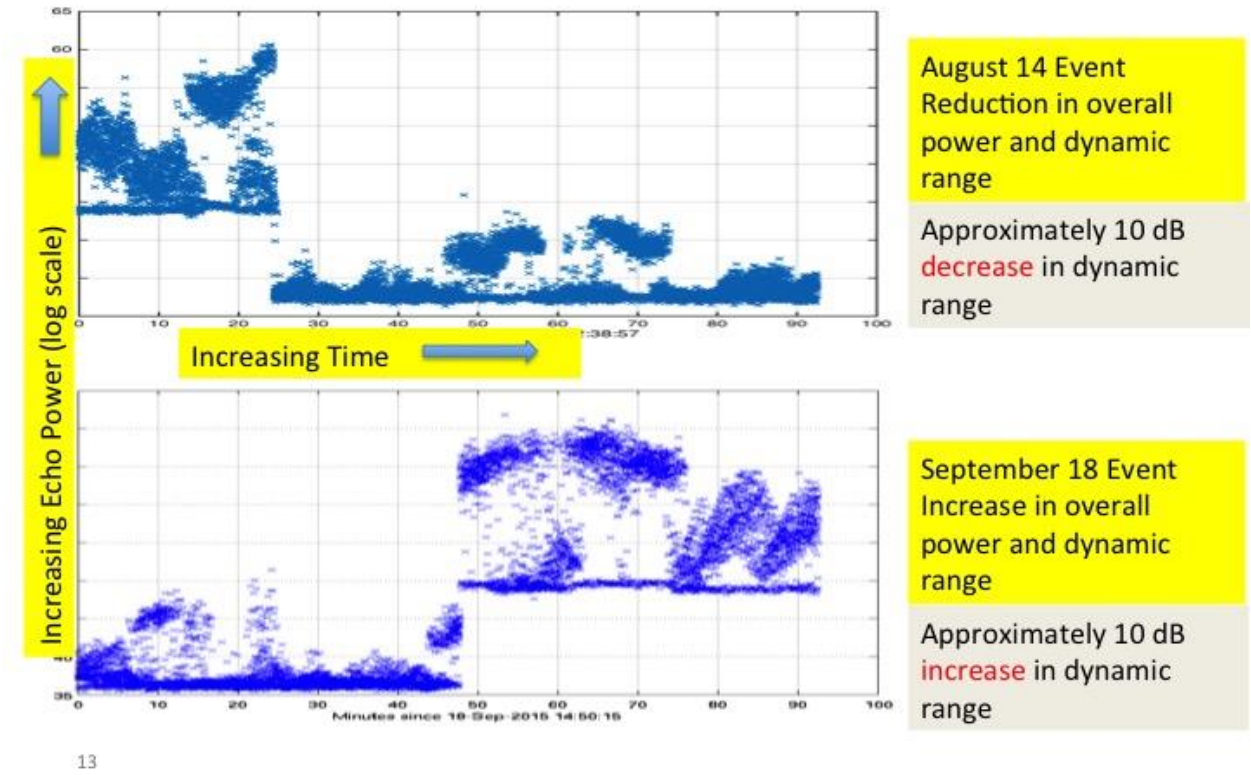

Figure 7.19. Graphical depiction of August 14 2015 anomaly and its reversal on Sept 18 2015. The y-axis on the plots are uncalibrated radar return power numbers. The x-axis is time in minutes. On the top panel we see the August 14 drop in power. Both the dynamic range of the values and the overall magnitude dropped. The Sept 18 reversal is shown on the bottom panel. On October 6, 2015, the anomaly reasserted itself and has persisted until now.

It was necessary to compute a constant offset in dB to recalibrate the data obtained in low SNR mode. In theory, if the loss in gain was fully monitored by the loop-back calibration scheme employed by the RapidScat radar such a recalibration would be unnecessary. Unfortunately, the magnitude of the loop-back calibration measurements has discrete jumps when the overall gain of the system is varied by tens of dB. Typically, a 10 dB attenuator setting is applied to keep the power measurements within the proper range for the analog to digital converter to properly quantize the full dynamic range of the signal. The loopback calibration measurement is properly handled for a 10 dB range of values for this attenuator setting. However, the anomaly applies an effective attenuation outside this nominal range and thus the values are rescaled. We observe similar behavior for QuikScat when the attenuator setting is varied beyond its normal range. To fix this issue it was necessary to apply a constant offset to the low SNR mode data. The correction (+14.45 dB) was computed by histogram-matching NRCS values from a week of data before the anomaly and a week of data after the anomaly. Figures 7.20-7.21 show how well the histograms of NRCS values match after the correction. After observing an additional 4 months of low SNR data, the calibration has been further refined to +14.15 dB. Whether or not this additional -0.3 dB bias represents a trend in the RapidScat data is still to be determined.

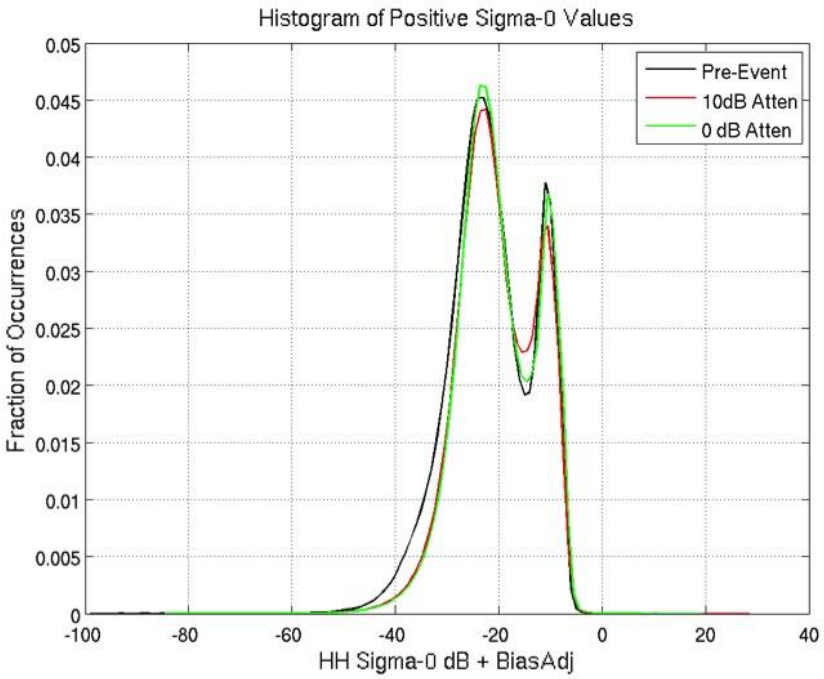

Figure 7.20. HH NRCS Histogram approximately one week of data before and after the anomaly. The black line is the before histogram. The green line is the after histogram with a 14.45 dB constant offset applied. The red line a special set of data obtained during the initial testing period right after the anomaly.

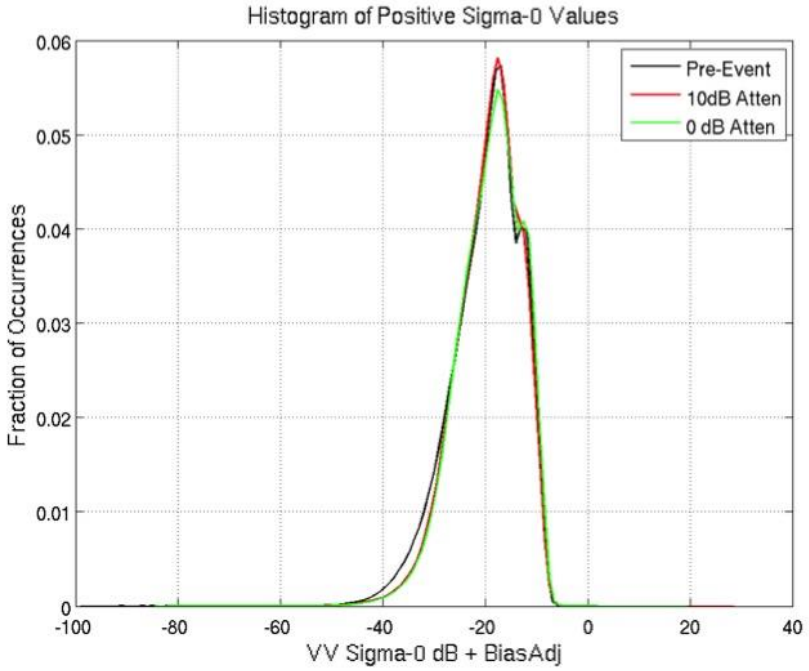

Figure 7.21. VV NRCS Histogram approximately one week of data before and after the anomaly. The black line is the before histogram.

7.5 Usefulness of RapidScat as a CDR

The RapidScat data prior to August 14, 2015 is of climate data quality and similar in all performance metrics to QuikScat data. There are only two areas where the high SNR mode data can be improved. First, the 0.25 dB NRCS offset needed to make wind retrievals consistent with the GMF should be applied. This improvement should also be made for QuikScat wind retrievals and a QuikScat footprint retrieved dataset should be developed for consistency. Second, further work needs to be done to correct the directional bias discontinuity in the middle of the RapidScat swath. Although this small (3-degree peak-to-peak) error does not affect overall wind statistics or trends it impacts wind derivative fields.

In addition to its utility as a CDR, RapidScat is also excellent in supporting CDRs from other scatterometers such as ASCAT or ScatSat as it provides close collocation data to:

- Serve as a bridge between instruments that make observations at different times of day
- Improve GMFs
- Improve Quality Control, i.e., rely on close ASCAT comparisons with much less rain for Quality Control tuning
- Improve consistency between C-band and Ku-band retrievals

The first point is arguably the most important case for RapidScat. RapidScat is the only instrument that makes consistently calibrated measurements at different local times of day. NWP models have proven insufficient to account for time-of-day differences in the winds. The insufficiency of NWPs is not surprising given that all the data they assimilate comes from various single local-time-of-day sensors with differences in calibration. The utility of RapidScat as a bridge between other sensors is further enhanced by the RapidScat orbit inclination. RapidScat obtains co-temporal, collocated measurements with all other satellites in the ocean wind vector constellation within every 90 minute orbit.

The low SNR mode RapidScat data that covers all but two weeks of the mission after August 14, 2015 is useful as a CDR and for supporting CDRs from other sensors. It has two shortcomings not present in the High SNR mode data: 1) noticeably increased speed and direction error for winds less than 5 m/s, and 2) slightly poorer rain flagging due to lack of brightness temperature measurements. Additional rain-flagging using radiometer rain observations can mitigate this shortcoming in the low SNR mode. In addition, the low SNR mode has not been in operation long enough to rule out an artificial trend in NRCS values. Despite these issues, for winds higher than 5 m/s and for bright rain forest (the prime target for cross-calibration) the performance is unlikely to be impacted. Six months to a year of additional RapidScat data will need to be analyzed to determine whether or not a trend exists. If so, it could likely be removed using comparisons with land NRCS over the Amazon or through the use of non-spinning QuikScat data